New insights into uranium stress responses of Arabidopsis roots through membrane- and cell wall-associated proteome analysis

Jonathan Przybyla-Toscano, Cherif Chetouhi, Lorraine Pennera, Yann Boursiac, Adrien Galeone, Fabienne Devime, Thierry Balliau, Véronique Santoni, Jacques Bourguignon, Claude Alban, et al.

New insights into uranium stress responses of Arabidopsis roots through membrane- and cell wall-associated proteome analysis

Jonathan Przybyla-Toscano[a], Cherif Chetouhi[a], Lorraine Pennera[a], Yann Boursiac[b], Adrien Galeone[a], Fabienne Devime[a], Thierry Balliau[c], Véronique Santoni[b], Jacques Bourguignon[a], Claude Alban[a], Stéphane Ravanel[a,*]

[a] Univ. Grenoble Alpes, INRAE, CNRS, CEA, IRIG, LPCV, 38000 Grenoble, France.

[b] Institute for Plant Sciences of Montpellier (IPSiM), Univ Montpellier, CNRS, INRAE, Institut Agro, Montpellier, France.

[c] PAPPSO-GQE-Le Moulon, INRAE, Université Paris-Sud, CNRS, AgroParisTech, Université Paris-Saclay, 91 190 Gif-sur-Yvette, France.

[*] Corresponding author

stephane.ravanel@cea.fr

Univ. Grenoble Alpes, INRAE, CNRS, CEA, IRIG, LPCV, 38000 Grenoble, France

Abstract

Uranium (U) is a non-essential and toxic metal for plants. In *Arabidopsis thaliana* plants challenged with uranyl nitrate, we showed that U was mostly (64-71% of the total) associated with the root insoluble fraction containing membrane and cell wall proteins. Therefore, to uncover new molecular mechanisms related to U stress, we used label-free quantitative proteomics to analyze the responses of the root membrane- and cell wall-enriched proteome. Of the 2,802 proteins identified, 458 showed differential accumulation (≥1.5-fold change) in response to U. Biological processes affected by U include response to stress, amino acid metabolism, and previously unexplored functions associated with membranes and the cell wall. Indeed, our analysis supports a dynamic and complex reorganization of the cell wall under U stress, including lignin and suberin synthesis, pectin modification, polysaccharide hydrolysis, and Casparian strips formation. Also, the abundance of proteins involved in vesicular trafficking and water flux was significantly altered by U stress. Measurements of root hydraulic conductivity and leaf transpiration indicated that U significantly decreased the plant's water flux. This disruption in water balance is likely due to a decrease in PIP aquaporin levels, which may serve as a protective mechanism to reduce U toxicity. Finally, the abundance of transporters and metal-binding proteins was altered,

suggesting that they may be involved in regulating the fate and toxicity of U in Arabidopsis. Overall, this study highlights how U stress impacts the insoluble root proteome, shedding light on the mechanisms used by plants to mitigate U toxicity.

Keywords: Uranium, *Arabidopsis thaliana*, root, proteome, cell wall, membranes, aquaporins

Highlights

- Uranium (U) accumulates mainly in the root insoluble fraction of Arabidopsis plants
- 458 proteins in the root insoluble fraction show differential accumulation in response to U
- U triggers a complex reorganization of the cell wall and Casparian strips
- Water flux and vesicular trafficking are significantly perturbed by U stress
- Several transporters and metal-binding proteins are regulated by U

Graphical abstract

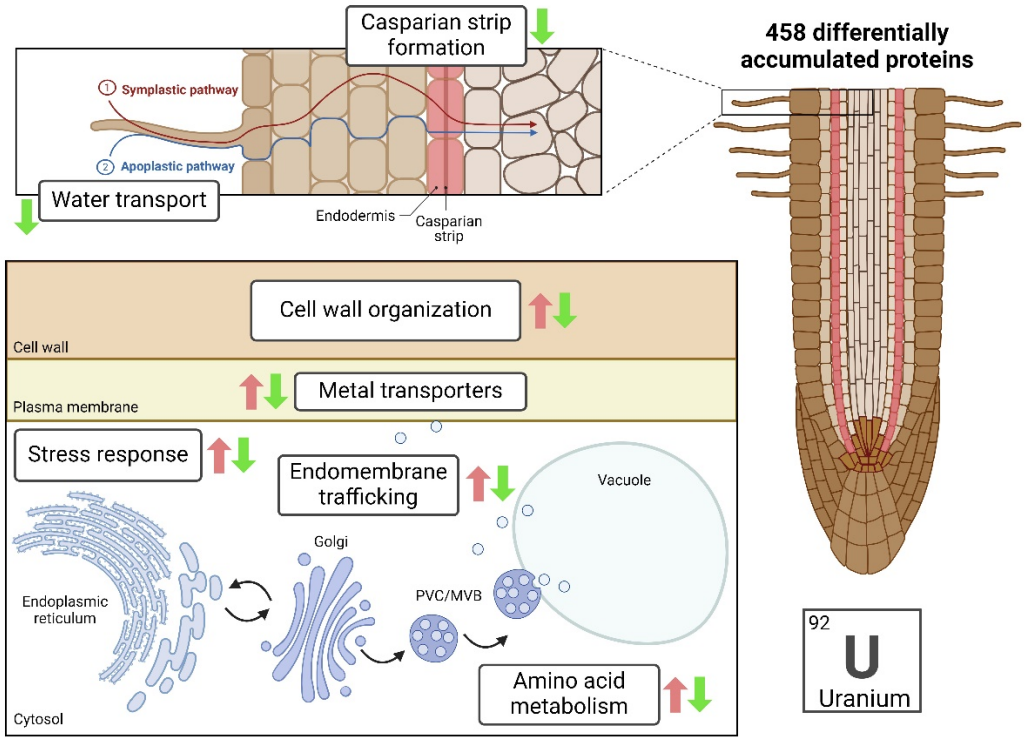

Abbreviations: DAP, differentially accumulated proteins; PIP, plasma membrane intrinsic protein.

1 - Introduction

Heavy metals are by nature present in the earth's crust composition. In addition, industrial and agricultural activities have direct consequences in their redistribution in the environment. This situation can lead to the accumulation of non-essential trace metals in the soil. As a result, metals are a threat to the environment and food safety due to their non-biodegradability, bioavailability and toxicity to crops. This is for instance the case for uranium (U). This actinide element is naturally dispersed in rocks and soils at an average concentration of 1-4 ppm [1]. It has also been found at high concentrations in a number of locations across the globe (see [2] for an overview). As examples, up to 250 mg $U.kg^{-1}$ were detected in sampling sites from Cunha Baixa U mine area in Portugal [3] and up to 3500 mg $U.kg^{-1}$ were detected in soils surrounding the reclaimed U mine of Rophin in France [4]. A field experiment conducted on edible vegetables grown in the agricultural area of Cunha Baixa showed that the amount of U in the edible tissues of lettuce, potato, green bean, carrot, cabbage, apple and maize were strongly increased [3,5]. In agricultural soils, U is also widely dispersed due to the extensive and long-term use of mineral fertilizers and the significant U contamination of phosphate ores [6]. In the environment, U coexists as U (+VI) and U (+IV) valence states and the uranyl ions (UO_2^{2+}) are the most abundant form of U in its oxidized state. In this form, uranyl cations react with inorganic anions or organic acids to form highly mobile and soluble complexes in the rhizosphere that are bioavailable and can be absorbed by plants [7].

Being sessile, plants have to cope with varying U concentrations in the environment, some of them being detrimental for growth. The chemical toxicity of U in plants has been analyzed in different species. In most species, U is mainly accumulated in roots and its translocation to aerial part is limited [2]. Analysis of the subcellular distribution of U from roots and protoplasts showed that this radionuclide is primarily sequestrated in the cell wall. In contrast, only small amounts of U was found in the cellular soluble fraction [8–10]. Uranium accumulation in plant tissues causes an inhibition of plant growth and root elongation, by interfering with carbon and nitrogen assimilation, photosynthesis, mineral nutrition (*i.e.* iron, calcium, phosphorus, magnesium), and hormone synthesis and distribution (*i.e.* auxin, jasmonic acid and salicylic acid) [10–18]. In addition, U exposure leads to an overproduction of reactive oxygen species (ROS) [17,19,20]. However, the molecular mechanisms behind these effects are still poorly understood. To date, the pathway for U entry in root cells is the best characterized. It was demonstrated that calcium-permeable channels are required for U uptake [21,22], while the main high affinity iron transporter IRT1 is dispensable in *A. thaliana* [23]. The calcium channel-dependent pathway for U uptake is conserved in yeast [24] and could represent a general uptake mechanism, at least in the eukaryotic lineage. In addition, the calcium concentration in the nutrient medium modulates U responses in shoots [25]. Beside transporter-mediated uptake, an additional pathway involving endocytic uptake might also be important for U transport into plant cells [26].

During the last decade, several comparative genomic approaches and/or quantitative analyses performed in *A. thaliana*, *Vicia faba* and *Ipomoea batatas* roots have provided insight into global gene expression and metabolic adjustments in response to U [8–10,13,20,27–29]. To shed light on the consequences of uranyl ions on the soluble proteome of Arabidopsis root and shoot cells, we previously developed an ionomic and top-down proteomic analysis coupled with biochemical and structural approaches [9,29]. In these studies, we identified 38 proteins able to bind U *in vitro* and we demonstrated that the Arabidopsis cation-binding protein PCaP1 is able to bind U(VI) in addition to other metals (*i.e.* Ca(II), Cu(II) and Fe(III) [29]. This newly identified U-binding protein, found in the plasma membrane or the cytosol, was originally known for its role in calcium signaling and its calcium-dependent regulation of the actin and the microtubule cytoskeleton [30,31]. While most of U is associated with insoluble cellular fractions, i.e. cell wall, membranes, and high-molecular-weight complexes [9], our knowledge of the effect of U on these cellular and extracellular structures is very limited. To date, the only documented example of a U-binding membrane protein in any organism is the bacterial UipA protein [32]. This single-pass transmembrane protein contains a large domain with nanomolar affinity for uranyl and Fe(III), and is essential for bacterial tolerance to the radionuclide.

In an effort to elucidate the molecular mechanisms underlying the chemotoxicity of U and the associated stress response in plants, the aim of this study was to identify membrane- and cell wall-associated proteins in Arabidopsis roots whose expression is regulated upon U stress. To this end, we have developed a label-free quantitative proteomic workflow based on nano-LC-MS/MS analysis followed by a detailed computational study. Using this approach, we analyzed the response of the Arabidopsis root membrane- and cell wall-enriched proteome under U stress and identified 458 differentially accumulated proteins. Our approach targeting the major site of U accumulation in root cells revealed unprecedented biological processes affected by the radionuclide, including cell wall organization, radial apoplastic transport, endomembrane trafficking, and water flux through aquaporins. Root hydraulic conductivity and leaf transpiration rate measurements confirmed that changes in water status in Arabidopsis under U stress could be an important mechanism to prevent U toxicity. Our analysis also highlighted potential transporters and metal-binding proteins involved in the fate of U in Arabidopsis.

2 – Material and methods

2.1 - Plant cultivation and uranium treatment

Arabidopsis thaliana Columbia-0 (Col-0) wild type (WT) seeds were initially sterilized and stratified in water for 3 d at 4°C. Plants were cultivated under hydroponic conditions at 20 °C and a relative humidity of 60% under a short-day photoperiod (8 h of light, 80 µmol photons m^{-2} s^{-1} photosynthetically active radiation) or a long-day photoperiod (16 h of light) in the case of transpiration and root hydraulic conductivity (Lp_r) measurements. For proteomic analysis and transpiration measurements, the experimental device described in [23] was used. Briefly, seedlings were placed on floating supports in black polypropylene containers filled with 200 mL of "Gre medium" (0.8 mM K_2SO_4, 1 mM $Ca(NO_3)_2$, 1 mM $MgSO_4$, 0.25 mM KH_2PO_4, 10 µM H_3BO_3, 0.2 µM $CuSO_4$, 2 µM $MnSO_4$, 0.01 µM $(NH_4)_6Mo_7O_{24}$, 2 µM $ZnSO_4$, 10 µM NaCl, 0.02 µM $CoCl_2$, 20 µM FeNaEDTA), pH 5.6, and cultivated for 30 d. Then, plants were transferred to distilled water supplemented or not with 5 µM or 50 µM uranyl nitrate ($UO_2(NO_3)_2$) during 48 h. At the end of the culture, excess of U was systematically removed from the root surface by a washing step with a carbonate solution (10 mM Na_2CO_3), followed by two additional washes with distilled water.

For root hydraulic conductivity measurements, 11 d-old seedlings grown in half-strength Murashige and Skoog agar medium were transferred on plastic plates floating over a basins filled with 8 L of hydroponic solution (1.25 mM KNO_3, 0.75 mM $MgSO_4$, 1.5 mM, $Ca(NO_3)_2$, 0.5 mM KH_2PO_4, 50 µM FeEDTA, 50 µM H_3BO_3, 12 µM $MnSO_4$, 0.70 µM $CuSO_4$, 1 µM $ZnSO_4$, 0.24 µM MoO_4Na_2, 100 µM Na_2SiO_3. Three weeks after germination, plants were transferred to the same culture medium depleted with KH_2PO_4 and Na_2SiO_3 to avoid any interaction with ($UO_2(NO_3)_2$). Uranyl nitrate treatment (50 µM) was applied for 24 h.

2.2 - Uranium quantification by Inductively Coupled Plasma Mass Spectrometry (ICP-MS)

For U determination, digestion of roots was performed at 90 °C during 4 h in 400 µL of 65% (w/v) HNO_3 (Suprapur, Merck) [23]. Proteins from the soluble and SDS-solubilized fractions were mineralized in 10% (w/v) HNO_3 for 2 h at 65 °C [29]. Mineralized samples were diluted in 0.65% (w/v) HNO_3 and U quantification was performed using an iCAP RQ ICP-MS (Thermo Fisher Scientific GmbH, Germany) operating in standard mode. The concentration was determined using a standard curve and a standard internal solution containing rhodium and ytterbium. The Qtegra software was used for data acquisition and integration.

2.3 - Protein extraction and quantification

Proteins were extracted from 400 to 700 mg (fresh weight) of roots. Root tissues were ground with liquid

nitrogen in a mortar before homogenization with the extraction solution (20 mM Tris-HCl, pH 7.0, 1 mM EDTA, 1 mM DTT and a cocktail of protease inhibitors, Roche). The suspension was ultracentrifuged at 105,000 *g* for 20 min. The supernatant containing the soluble proteins was collected, while the pellet was washed twice with the extraction solution and then resuspended in the extraction solution supplemented with 1% (w/v) SDS. The suspension was incubated at 4 °C for 30 min to allow protein solubilization by SDS and then centrifuged at 15,000 *g* for 20 min. The supernatant was collected to recover proteins solubilized by SDS. Protein quantification of the extracts was estimated using the Pierce BCA Protein Assay kit (Thermo Scientific) and bovine serum albumin as standard.

2.4 - SDS PAGE immunoblot assay

Soluble and SDS-solubilized proteins from root extracts were separated on 12% (w/v) reducing polyacrylamide gels (SDS-PAGE) and transferred onto nitrocellulose or PVDF membranes. After a blocking step with 4% (w/v) BSA in TBS-0.1% (v/v) Tween, the immunoblot reaction was performed overnight at 4 °C with polyclonal antibodies raised against the membrane tonoplast intrinsic protein (TIP1;1, TIP1;2) (Agrisera AS09493),the soluble fructose-bisphosphate aldolases (FBAs) [33], or the U-binding proteins PCaP1 [29] and GRP7 [34]. Following three washes, membranes were incubated during 1 h at room temperature with secondary antibodies conjugated to horseradish peroxidase. Signal detection was performed using the ECL prime detection reagent (Amersham) and fluorescence was visualized using ImageQuant 800 (Amersham) imaging system.

2.5 - Proteomic preparation and label-free nanoLC-MS/MS analysis

About 15 µg of proteins were separated on SDS-PAGE gels (Bio-Rad 3450009) at a constant voltage of 200 V for 12 min. Gels were stained with the Bio-Safe™ Coomassie Stain solution (Bio-Rad 1610786) according to the manufacturer recommendations. Proteins were fixed with a 10% (v/v) acetic acid and 40% (v/v) ethanol solution, and rinsed with distilled water. After acquisition of a gel image, the tracks were cut into three bands corresponding to the three protein subfractions. The bands were rinsed and digested with 200 ng trypsin in a final volume of 100 µL. After digestion, samples were dried using a SPD111 SpeedVac (Thermo Scientific) until complete evaporation. LC-MS/MS analyzes were performed using a NanoLC-Ultra system (nano2DUltra, Eksigent) connected to a Q-Exactive plus mass spectrometer (Thermo Electron, Waltham, MA, USA). For each sample, approximately 400 ng of the peptides were loaded onto a Biosphere C18 120 Angstrom precolumn (2 cm, 100 µm, 5 µm; nanoseparation) at 7,500 nL min^{-1} and desalted with 0.1% (v/v) formic acid and 2% (v/v) acetonitrile. After 5 min, the precolumn was connected to a Biosphere C18 120 Angstrom nanocolumn (30 cm, 75 µm, 3 µm; nanoseparation). The gradient profile contained 5 steps corresponding to: step 0 (0 min in 95% buffer A [0.1% (v/v) formic acid] and 5% buffer B [0.1% (v/v) formic acid in acetonitrile]), step 1 (75 min in 70% buffer A and 30% buffer B), step 2 (80 min in 5% buffer A and 95% buffer B), step 3 (85 min

in 5% buffer A and 95% buffer B), step 4 (88 min in 95% buffer A and 5% buffer B) and step 5 (95 min in 95% buffer A and 5% buffer B). Nano-ESI was performed with a spray voltage of 1.6 kV and a heated capillary temperature of 250 °C. The acquisition was performed using XCalibur 4.0.29 (Thermo Electron) software in data-dependent mode with the following steps: (1) full MS scan was acquired at 75.000 of resolution with an AGC target to 3*106 in a maximum of 250 ms for mass range of 350 to 1400 m/z; (2) MS/MS scan was acquired at 17.500 of resolution with an AGC target of 1*105 in a maximum of 120 ms and an isolation window of 1.5 m/z. Step 2 was repeated for the 8 most intense ions in the full scan (1) if the intensity was greater than 8.3*103 and the charge was 2 or 3. The peptide match option was set to on and isotopes of the same ion were excluded. Dynamic exclusion was set to 50 s.

2.6 - Data analyses and protein identification

Data files were converted to open source mzXML format using msConvert software from the ProteoWizard 3.0.9576 package [35]. During conversion, the MS and MS/MS data were centered. *Arabidopsis thaliana* protein database (Araport11) was used as a reference for protein identification. A contaminant database containing the sequences of standard contaminants such as trypsin, keratin, and serum albumin was also queried. Search was performed using X!Tandem (version Piledriver 2015.04.01.1) [36]. Trypsin was set in strict mode with 1 miscleavage in the first step. Carbamidomethylation of cysteine was set as a fixed modification. Oxidation of methionine, excision of N-terminal methionine, with or without acetylation, and pyroglutamate from glutamine or glutamic acid were set as potential modifications. In a second pass, the maximum allowed miscleavage was set to 5, deamidation on asparagine and glutamine and oxidation of tryptophan were added to the list of potential modifications.

Proteins were filtered and sorted using X!TandemPipeline (version 0.4.17) [37]. Each identified protein was validated by the presence of at least two peptides with an E-value <0.01 and a protein E-value $<10^{-5}$. According to these parameters, results were filtered to an estimated false discovery rate (FDR) of 0.15% at the peptide level and 0% at the protein level. The identified peptides were quantified by eXtracted Ion Current (XIC) and MassChroQ software (version 2.2.22) [38] using the following alignment parameters: ms2_1 alignment method tendency_halfwindow of 10, ms2_smoothing_halfwindow of 15, ms1_smoothing_halfwindow of 0. The quantification method XIC was based on max, min and max ppm range of 10, anti-spike half of 5, mean filter half_edge of 2, minmax_half_edge of 4 and maxmin_half_edge of 3. The thresholds for detection were 30,000 for min and 50,000 for max. The mass spectrometry proteomics data (**Table S1)** have been deposited to the ProteomeXchange consortium via the PRIDE partner repository (https://www.ebi.ac.uk/pride/) with the dataset identifier PXD048867.

2.7 - Peptide and protein normalization and quantification

The intensity of each peptide in each sample was normalized using a median-based method taking into consideration the peptide intensities of reference samples. The reference samples correspond to the pool of peptide ions extracted from the 18 samples analyzed using the same pipeline. Proteins were then quantified after removing common and doubtful peptide ions, peptides with too many missing data (more than 10%), and peptides whose intensity profile deviated from the average profile of peptide-mz (correlation less than 0.5). Missing values at the peptide level were imputed using the Iterative Robust Model-based Imputation method (R package VIM) [39]. Proteins represented by at least two reproducible and consistent peptides were quantified. Relative protein abundance was calculated as the sum of XIC intensities of selected peptides and log10 transformed (**Table S2)**. For proteins that were not detected in one of the samples, the intensity was imputed using the minimum intensity measured in the experiment.

2.8 - Statistical, protein clustering and bioinformatics analyses of identified proteins

The results were analyzed using the program MCQR (version 0.5.2)**.** Proteins regulated by U treatment were identified using a one-way analysis of variance (ANOVA) with the following linear model: $Y_{ij} = \mu + U_i + \varepsilon_{ij}$, where Y_{ij} refers to individual protein abundance, μ is the general mean, U_j is the effect of U, and ε_{jk} is the residual. For each protein, the *p*-value obtained from the ANOVA test was adjusted (*Padj* < 0.05). Proteins that showed *Padj* <0.05 in the ANOVA were subjected to a Tukey test to identify proteins that showed differential accumulation in at least one of the three comparisons (U5 versus U0, U50 versus U0, and U50 versus U5) with *p*-value < 0.05 (**Table S3**). A 1.5 fold-change threshold was then used to select proteins whose abundance was significantly affected by U stress.

The Self-Organizing Tree Algorithm (SOTA) of the identified proteins was performed using the Z-score transformed values (R package SOTA) [40]. Eight clusters were selected to describe the more representative protein accumulation patterns in the three conditions (**Table S4**). In **Table S5**, the AGI code, UniProt ID, gene name(s), gene description(s) for each identified protein were retrieved from the Araport 11 (Arabidopsis information resource (https://www.arabidopsis.org/) or UniProtKB databases. Protein classes were compiled from PantherDB (http://www.pantherdb.org/; last update February 23, 2022), whereas enzyme families were provided from Gene Ontology (GO) “molecular function” annotations available through QuickGO (www.ebi.ac.uk/QuickGO/) coupled with a manual curation (**Table S6**). The nature of (putative) metallic cofactors was obtained from the UniProtKB database (https://www.uniprot.org/). Predicted or experimentally proven subcellular localizations of proteins were compiled from the resource SUBAcon (SUBcellular Arabidopsis consensus v5; http://SUBA.live; last update June 30, 2022) [41].

Hierarchical clustering was generated for the proteins that showed significant variation under U exposure using the Heatmapper web application [42]. The Cytoscape v3.9.1 plugin Biological networks

gene ontology (BiNGO) v3.0.3 [43] and the Metascape software (https://metascape.org) [44] were used to calculate GO term enrichment of regulated proteins. The analysis was conducted using the default BINGO settings with the Bonferroni family-wise error rate correction (with significant level set at <0.05) and the *Arabidopsis thaliana* annotation. Bubble plots were generated with SR plot (https://www.bioinformatics.com.cn/en). For relevant positioning in metabolic pathways, proteins were analyzed using the Arabidopsis metabolic network knowledge database ChloroKB [45].

2.9 –Root hydraulic conductivity and transpiration measurements

Measurement of root hydraulic conductivity ($L p_r$, in mL g^{-1} h^{-1} MPa^{-1}) was performed using a pressure chamber coupled to a flowmeter as described in [46]. Excised roots were pretreated at 350 kPa for 10 min and pressure (P)-induced sap flow (J_v) was measured consecutively at 320, 160 and 240 kPa. Then, 2 mM of sodium azide (NaN_3) was applied for 30 min and J_v was recorded. Root dry weight (DW_r) was measured after dehydration at 80 °C for 48 h and $L p_r$ of an individual root system was calculated from the equation: $L p_r = J_v/P/DW_r$. For transpiration measurements (water loss; g H_2O cm^{-2} and g H_2O h^{-1} cm^{-2}), plants were weighed every 3.5 h from the beginning to the end of the photoperiod throughout the treatment period. Foliar surface was determined using the ImageJ software.

3 - Results

3.1 - Uranium is preferentially bound to membrane-associated and other insoluble proteins in roots

To gain insights into the responses of the root proteome under U stress, 30-day-old *Arabidopsis thaliana* (Col-0) plants were challenged with 5 and 50 µM uranyl nitrate for 48 h, thereafter referred to as U5 and U50 conditions, respectively. Uranyl nitrate was provided in distilled water in order to limit U interaction with other mineral components (*e.g.* phosphate) and maximize its absorption by roots [13,22,47]. Roots treated with 5 and 50 µM uranyl nitrate accumulated 135 ± 23 and 1609 ± 157 µg U per g fresh weight, respectively (mean ± SD, n=6 biological replicates) (**Figure S1**). In shoots, U concentration was much lower (0.4 ± 0.1 and 2.2 ± 1.4 $\mu g.g^{-1}$ FW in U5 and U50 plants, respectively), in agreement with the low translocation rate of U observed in Arabidopsis in these conditions [11,22,23,48]. Total proteins were extracted from root tissues and soluble proteins were separated from insoluble material by ultracentrifugation. Then, membrane-bound and other insoluble proteins were extracted in the presence of 1% (w/v) SDS and recovered from residual insoluble material by centrifugation. Immunoblot analysis with antibodies against the membrane integral tonoplast protein (TIPs) and the soluble fructose 1,6-bisphosphate aldolase isoforms (FBAs) was performed to assess the quality of protein fractions. TIPs were detected only in the SDS-solubilized fraction, whereas aldolases were detected only in the soluble fraction (**Figures 1A, S2 and S3**). This result confirms the specific enrichment of the two fractions in

either soluble or membrane-associated proteins with very low cross contamination. In the soluble fraction, the amount of U determined by ICP-MS was 0.20 ± 0.05 and 3.02 ± 1.16 µg. mg^{-1} protein in the roots of U5 and U50 plants, respectively (**Figure 1B**). The amount of U in membrane-associated and other insoluble proteins was about 10 to 15-time higher, with 3.1 ± 1.0 and 28.1 ± 3.6 µg U per mg protein (**Figure 1B**). Considering the amount of proteins recovered in the soluble and SDS-solubilized fractions (13 ± 2 % and 87 ± 2%, respectively), it can be calculated that two-thirds of the total U was associated with the SDS-solubilized fractions (64 ± 7 % and 71 ± 6 % for U5 and U50, respectively), with the remainder in the soluble fraction (**Figure 1C**). This result is in agreement with previous data obtained in Arabidopsis cell suspension cultures treated with uranyl nitrate, in which most of U in the protoplasts was associated with membranes [9]. It also suggests that the function and/or abundance of membrane-associated and other insoluble proteins may be particularly compromised under U stress. For these reasons, we focused our analysis on the responses of the root insoluble proteome to U stress.

3.2 - The root membrane- and cell wall-enriched proteome is strongly affected by uranium

SDS-solubilized protein fractions from roots of the control (U0), U5 and U50 conditions were analyzed by nano-LC-MS/MS using a Q-Exactive mass spectrometer (n=6 biological replicates per condition). The analysis allowed the identification of 29,371 peptides corresponding to 3,462 indistinguishable protein groups (validated by at least 2 peptides with E-value<0.01, and a protein E-value<10^{-5}) (**Table S1**). Within this dataset, 2,802 proteins (corresponding to 17,730 peptides) were quantified in a reproducible manner using a XIC-based approach (**Table S2**). The subcellular localization of the 2,802 proteins was analyzed using two complementary tools for gene ontology (GO) enrichment analysis, the BiNGO plugin of Cytoscape and the Metascape software for *A. thaliana*. With Metascape, enrichment clustering eliminates confounding data interpretation issues that can arise from redundancies in descriptors and ontologies, facilitating interpretation of results with relatively small clusters that cannot be identified with BiNGO. The BiNGO analysis indicated that the most enriched (from 4- to 10-fold) subcellular compartments in the insoluble proteome are the peroxisome, plasma membrane, cell wall, endosome, nucleolus, vacuole, endoplasmic reticulum (ER), and nuclear envelope (**Figure S4A**). In addition, the Metascape cellular component enrichment analysis indicated that several protein complexes and vesicular systems were significantly enriched in this fraction (**Figure S4B**). Together, these results showed that the SDS-solubilized protein fraction from roots is enriched in membrane proteins from different subcellular compartments, in cell wall-associated proteins (enrichment >3.5), and in protein complexes (enrichment >3). This fraction is now referred to as the root membrane- and cell wall-enriched proteome, or simply the root membrane proteome.

Using a 1.5-fold change threshold for biological significance, we identified 458 differentially accumulated proteins (DAPs) in the root membrane proteome under U stress (ANOVA, *p*-value <0.05) (**Table S3**). As

shown in Volcano plots and Venn diagram (**Figure S5**), a total of 68 proteins changed significantly in the comparison between U0 and U5 treatments (49 up-accumulated, 19 down-accumulated), 343 proteins changed between U0 and U50 (168 up-accumulated, 175 down-accumulated), and 299 proteins changed between U5 and U50 (143 up-accumulated, 156 down-accumulated). Overall, this indicates that most of the 458 DAPs were deregulated by the high U concentration (U50), whereas lower U stress (U5) moderately interfered with the root membrane- and cell wall-enriched proteome. To refine this comparison, hierarchical clustering analysis of the 458 DAPs clearly confirmed the grouping of biological replicates (n=6) for each U treatment (**Figure S6**). For each of the three conditions, a specific pattern of protein accumulation was observed. The root membrane proteome from plants cultivated in U0 and U5 conditions segregated drastically from that of U50. Finally, a self-organizing tree algorithm (SOTA) analysis was used to define eight clusters of proteins based on their accumulation patterns in response to U concentrations in the medium (**Figure 2; Table S4**). Clusters 1 and 2 included proteins that preferentially accumulated as the U concentration increased. In contrast, clusters 4 and 5 contained proteins whose abundance decreased with increasing U concentrations. Clusters 3, 6, 7 and 8 grouped proteins with opposite abundance patterns at the two U concentrations. Approximately half of the 458 DAPs were up-accumulated in response to U50 (clusters 1-3), whereas the abundance of the remaining 50% proteins was decreased in this condition (clusters 4-6) (**Figure 2**).

3.3 - Membrane- and cell wall-associated proteins regulated by uranium perform a wide range of molecular functions

To further delineate whether some cell compartments are specifically impacted by U stress, the subcellular localization of the 458 DAPs was analyzed using the BiNGO and Metascape tools. The plasma membrane, ER, vacuole, and cell wall were the most enriched subcellular compartments in the BiNGO analysis (>3.5-fold enrichment) (**Figure 3A**). Additionally, the supramolecular complex, secretory vesicle, Golgi cisterna, and Casparian strip terms were overrepresented in the Metascape analysis (>3-fold enrichment) (**Figure 3B**). Altogether, these results suggest that U influences the abundance of proteins distributed in most of the cell compartments, and support an enrichment of the cell wall and membrane fractions. A moderate enrichment (2.7-fold) of proteins detected in the cytosol may reflect the presence of protein complexes that interact, at least transiently, with the membranes.

We investigated the predicted molecular functions of the 458 DAPs under U stress. Proteins were grouped into functional classes based on GO annotations related to the molecular function and data were manually curated. Our analysis showed that enzymes represented 46% of U-accumulated proteins (**Figure 4A**; **Table S6**). The other proteins belonged to the classes of transporters (13%), transcriptional/translational factors (9%), chaperones/co-chaperones (6%) or transmembrane receptors (4%), while 24 proteins (5%) had other functions and 89 proteins (19%) were referred to as “unknown” (**Figure 4A; Table S5**). Focusing on the enzyme class, hydrolases, oxidoreductases and transferases

were mainly identified, while lyases, ligases and isomerases accounted for a smaller proportion (**Figure 4A; Table S5**). The hydrolase protein class included proteases, phosphatases, glycosidases, esterases, lipases, nucleases and helicases (**Table S5**). Oxidoreductases were primarily represented by peroxidases. Finally, kinases, transaminases and aldolases formed the transferase class. Concerning transporters, families involved in the transport of nucleotides, proteins, vesicles, water, sugars and metals were regulated by U (**Table S5**). Notably, more than 30% of the proteins identified in our proteomic analysis were annotated as metalloproteins (**Figure 4B**). The abundance of genuine or predicted iron-, calcium-, zinc-, and magnesium-containing proteins was noticeably affected by U (**Figure 4B**).

3.4 - Multiple biological pathways involved in stress response, metabolism and cell organization are modified by uranium

To gain insight into the biological processes regulated by U, we performed an enrichment analysis of the 458 DAPs using BiNGO and Metascape. For biological process enrichment analysis, the Metascape tool has the advantage of identifying GO constituted by a smaller set of proteins compared to BiNGO. Among the most enriched (>1.8-fold) biological processes, considering only higher levels in the GO term hierarchy, the terms response to stress (GO:0006950), response to metal ion (GO:0010038), amino acid metabolic process (GO:0006520), monocarboxylic acid metabolic process (GO:0032787), and transport (GO:0006810) were identified using BiNGO (**Figure 5A**). The analysis using Metascape revealed additional enriched (>2.2-fold) biological processes such as protein folding (GO:0006457), tRNA aminoacetylation (GO:0043039), phenylpropanoid metabolic process (GO:0009698), cell wall organization (GO:0071555), and cell-cell junction assembly (GO:0007043) (**Figure 5B**). This analysis indicates that multiple biological processes are affected in response to U. In the following paragraphs, we provide a detailed description of the molecular components associated with the GO terms and their sub-terms. To provide a clear overview of the effects of U on the root membrane proteome, we have grouped these terms/sub-terms into three main categories, namely (i) stress, (ii) metabolism and cell wall organization, and (iii) transport and compartmentalization.

Stress -The stress category includes the GO terms response to stress (and its child term response to oxidative stress, GO:0006979), protein folding, and response to metal ions. Response to stress is one of the largest GO biological process with 75 DAPs mainly present in clusters CL1, CL3, CL4 and CL6 (**Figure 2**). Among them, 23 proteins constitute the sub-group response to oxidative stress (**Figure 6A**). Only a few of these proteins were accumulated upon U stress (CL1 and CL3), including plastidial peroxiredoxin PRXIIB and PRXIIE, mitochondrial peroxiredoxin PRXIIF, glutathione peroxidase 6 (GPX6), thioredoxin H type 5 (TRX5), and peptide methionine sulfoxide reductase 4 (PMSR4). All other proteins in this group were less abundant in the presence of U50, such as the cytosolic and plastidial

copper/zinc superoxide dismutase 1 and 2 (CSD1/2), gamma-glutamyl transpeptidase 1 (GGT1), and up to 13 class-III peroxidases (PRXs) (**Figure 6A**). The second GO sub-group, protein folding, comprised a dozen proteins that accumulate in response to U (CL1 and CL3), of which several chaperones/chaperonins and three peptidyl-prolyl cis-trans isomerases (ROC1/3/5). Finally, many of the DAPs involved in response to stress (at least 32 proteins) are metalloproteins and/or proteins regulated by metal ions. In addition to the numerous PRXs and CSDs already described above, this group contains a number of proteins involved in the response to biotic and abiotic stress and/or metal homeostasis. Among the up-accumulated proteins, the calcium-binding chaperone calreticulin-3 (CALR3) [49], the calcium-, zinc- and iron-binding early response to dehydration 10 and 14 proteins (ERD10/14) [50], the nickel-binding phosphorylated protein 34 (PHOS34) [51], as well as the cadmium- and zinc-responsive pre-mRNA regulatory protein glycine-rich protein 7 (GRP7) [52,53] were found. In contrast, the chloroplastic iron storage protein ferritin 1 (FER1) [54] and the plasma membrane-associated cation-binding protein 1 (PCaP1) [31,55] were present at lower levels under U stress. To support these data, we analyzed the steady-state levels of the GRP7 and PCaP1 proteins in the roots of Arabidopsis plants challenged with U by immunoblot. Results shown in **Figure 7** confirm that the abundance of these two U-binding proteins [29] is modified by U stress and that the accumulation profiles determined by immunolabeling fit well with XIC-based quantitative proteomic data.

Metabolism and cell wall organization - Several terms related to plant metabolism and cellular organization are significantly enriched among the 458 DAPs. They include amino acid metabolic process (and its sub-term branched chain amino acid metabolic process, GO:0009081), monocarboxylic acid metabolic process, tRNA aminoacetylation, phenylpropanoid metabolic process, cell wall organization, and cell-cell junction assembly (**Figure 5**). These proteins are distributed in all eight clusters from the SOTA analysis, but are mainly present in CL1, CL3, CL4, and CL6. The GO term amino acid metabolic process includes enzymes involved in the synthesis of several amino acids (**Figure S7**). The synthesis of branched-chain amino acids (BCAA; Ile, Leu, Val) is particularly impacted by U stress with the accumulation of four enzymes catalyzing consecutive steps, namely acetohydroxy acid synthase (ALS), acetohydroxy acid isomeroreductase (ILV5), dihydroxyacid dehydrate (DHAD), and isopropylmalate synthase (MAML-4) (**Figure S7**). In contrast, the isopropylmalate isomerase 2 (IPMI2), methylthioalkylmalate synthase 3 (MAM3), superroot (SUR1) and cytochrome 5B-C proteins involved in the biosynthetic pathway of BCAA-derived aliphatic glucosinolates are less abundant [56]. The synthesis of aromatic amino acids (Phe, Tyr, Trp), aspartate-derived amino acids (Thr, Lys), amino acids contributing to one-carbon metabolism (Ser, Gly, Met), and Arg are also up-accumulated in response to U50 (**Figure S7**). The highest concentration of U also has a significant effect on tRNA aminoacetylation reactions as observed by the accumulation of eight aminoacyl tRNA-ligases (**Figure S7**), suggesting an effect of the radionuclide on *de novo* protein synthesis. In connection with aromatic amino acid

synthesis, the response to U stress is characterized by the differential accumulation of enzymes belonging to the phenylpropanoid metabolic process. Two enzymes involved in the activation of phenylpropanoid precursors, coumarate CoA ligase (4CLL7) and cinnamyl alcohol dehydrogenase (CAD5), accumulated during U stress (**Figure 6B**), suggesting an increased synthesis of flavonoids or monolignols [57]. Following their transport to the cell wall, monolignols are oxidized by members of the large family of class-III peroxidases and further polymerized to form lignin. As mentioned before, 13 class-III peroxidases predicted to be extracellular were decreased in abundance in response to U exposure (**Figure 6A**), suggesting a significant effect of U on the homeostasis of this major cell wall polymer. In addition, important changes in cell wall composition are supported by several proteins whose abundance changes during U stress. First, the abundance of enzymes involved in the modification of pectin, namely pectin methylesterases (*i.e.* PME1/17/18) and pectin acetylesterase 11 (PAE11), is decreased in response to U stress (**Figure 6B**). Second, enzymes involved in either suberin synthesis (*e.g.* long chain acyl-CoA synthetase LACS2, cytochrome P450 86A1, feruloyl-CoA transferase HHT1) [58] or the degradation of cell wall polysaccharides (glycoside hydrolases acting on diverse substrates, *i.e.* alpha and beta-galactoside, beta-glucoside, xyloglucan, fructan) [59] are either more or less abundant in U5 and U50 than in control samples (**Figure 6B**). These important changes in cell wall-organizing enzymes suggest a dynamic and complex reorganization of the cell wall in response to U stress. This assumption is strengthened by the observation that the abundance of four Casparian strip membrane proteins (*i.e.* CASP1-4) and uclacyanin 2 (UCC2), both involved in the Casparian strip formation and consequently in cell-cell junctions [60–62], was decreased in the presence of U50 (CL4 in **Figure 2**, **Figure 6B**).

Transport and compartmentalization - The transport group, formed by the enriched GO term transport and its child terms vesicle-mediated transport (GO:0016192) and water transport (GO:0006833), contains 47 DAPs associated with CL1, CL2 and CL6 (**Figure 2**). The child terms vesicle-mediated transport and water transport were enriched up to 4- and 22-fold, respectively, according to the BiNGO and Metascape analyses (**Figure 5**). An important regulation of the endomembrane trafficking pathways in response to U is suggested by the differential accumulation of the prenylated Rab acceptors PRA1 (*i.e.* PRA1.B1/F3/F4), the β'1 subunit of the COP1 coat, the transport protein particle C5 (TRAPPC5) subunit of the TRAPP I complex, and the Sec1/Munc18 protein SLY1 (**Figure 6C; Figure S8**). All these proteins mediate the vesicle transport between the ER and the Golgi apparatus. Acting downstream, the TOM1-like protein 6 (TOL6) and some ESCRT-III-related components, including the sucrose non-fermenting 7.1/7.2 (SNF7.1/7.2), vacuolar protein sorting 2.1/46 (VPS2.1/46), and alg-2 interacting protein-x (ALIX) were accumulated upon U stress. Only the abundance of TOL6 was reduced at U50. These sequential ESCRT complexes orchestrate the biogenesis of multivesicular body (MVB) and the sorting of ubiquitinated cargo proteins for vacuolar degradation [63]. The abundance of other proteins

involved in the post-Golgi trafficking were accumulated during U stress, including the vacuolar-sorting receptor 1 (VSR1), and the SNARE proteins YKT61 and SYP122 (**Figure 6C; Figure S8**).

The accumulation of solute transporters is also modified by U stress (**Figure 6D**). Among transporters likely to transport metals, the zinc transporters MTPA2, PCR2 and HIPP25 were down-accumulated under U50 whereas the At5g52680 and At5g52710 proteins annotated as copper transporters were up-accumulated under these conditions (**Figure 6D**). The ABCB1, ABCB11, ABCC2, and ABCF1 members of the ABC transporter family, related to metal homeostasis, were specifically accumulated under different U concentrations (**Figure 6D**). Concerning water transport, eight aquaporins, most of which belong to the plasma membrane intrinsic protein (PIP) subfamily, were down-accumulated in the presence of a high concentration of U (**Figure 6D**).

3.5 – Uranium alters plant water status via an aquaporin-dependent process

To gain functional insights into the decrease accumulation of several aquaporins, we investigated the water status of Arabidopsis plants challenged with U. Water transport in Arabidopsis roots is considered to be mainly contributed by aquaporins of the PIP subgroup [64]. To assess potential interference between U and aquaporin function, root water transport capacity was characterized by measuring the root hydraulic conductivity (L_{p_r}) of WT plants treated with 50 µM uranyl nitrate. As shown in **Figure 8A**, 24 h of U treatment caused a three-fold decrease in L_{p_r} compared to the control. Then, excised root systems were treated with NaN_3, an inhibitor of aquaporin activity [64,65]. As previously observed, the overall L_{p_r} was greatly dependent on an aquaporin-related component under control conditions. Under U treatment, however, only a slight inhibition of L_{p_r} upon NaN_3 addition was observed, indicating that the aquaporin-related fraction was already strongly reduced (**Figure 8A**). These observations showed that aquaporin function in Arabidopsis roots is already severely impaired when exposed to U, leading to reduced efficiency of the aquaporin inhibitor under U stress. Beyond root hydraulics, we then analyzed whether U could affect the hydraulic status of the whole plant. For this purpose, leaf transpiration rate was measured in plants cultivated in the presence of 50 µM uranyl nitrate for 48 h. In line with the L_{p_r} results, the transpiration rate in U-treated plants decreased by nearly 50% from 24 h of treatment when compared to untreated plants (**Figure 8B**). Altogether, these results demonstrate a reduced aquaporin-dependent water flux in roots and shoots under U stress conditions, which correlates well with the down-accumulation of several PIP proteins (**Figure 6D**).

4 - Discussion

4.1. Uranium interferes with the accumulation of numerous metal-binding proteins, including enzymes responsible for ROS scavenging

Although proteomics has been widely used to characterize plant responses to heavy metal stress (for a

review see [66]), limitations of the methods have hindered the identification of low abundant proteins with potential roles in these processes. To address some of these limitations, current deep proteome profiling methods rely on fractionation and protein enrichment steps. In this study, XIC-based quantification of the membrane- and cell wall-enriched proteome of Arabidopsis roots identified 2,802 proteins and showed that the abundance of 458 of them was significantly changed during U stress (fold change >1.5, p <0.05). The two high-affinity uranyl-binding proteins identified so far in Arabidopsis, PCaP1 and GRP7 [29,34], are present among the 458 DAPs and their behavior in response to U stress was confirmed by immunoblot analysis (**Figure 7**). This finding supports the idea that the insoluble fraction of the root proteome, as the primary site of U accumulation (**Figure 1**), is a key compartment for analyzing the consequences of U intoxication and uncovering new defense mechanisms. About 30% of the identified DAPs are genuine or putative metalloproteins (**Figure 4**). This figure per se does not reflect an enrichment in metal-containing proteins as it is commonly estimated that one-third of proteins require metals, of which magnesium is the most common [67]. Yet, our analysis indicates that the abundance of iron- and calcium- containing proteins is the most affected by U (**Figure 4**). This observation corroborates previous data showing a preferential interference between U and iron or calcium homeostasis in plants [13,22,23,25]. One of the explanation would be that uranyl ions compete and displace iron and calcium in some proteins, as observed in the eukaryotic transferrin and calmodulin proteins [68,69]. The release of free iron triggered by U could lead to oxidative stress. In line with this hypothesis, a set of antioxidant enzymes and chaperones related to oxidative stress was significantly modified upon U stress (**Figure 6A**). An increase of ROS species has already been observed in the roots from plants challenged with U [16,19,20,70,71].

4.2. Amino acids and their derivatives could be key players in U scavenging and tolerance

An important deregulation of amino acid metabolism in response to U stress was highlighted during this analysis (**Figure 5; Figure S7**). However, it is important to note that analyzing the root membrane- and cell wall-enriched proteome provides only a partial perspective on amino acid metabolism. This process is primarily soluble, but it also involves multienzyme complexes, such as metabolons, or membrane-associated proteins [72]. An interaction between nitrogen metabolism and U has been previously described in plants, and a metabolomic analysis of *Vicia faba* roots showed that U significantly reduced the content of various free amino acids [8,10]. Our proteomic analysis revealed that several enzymes involved in the synthesis of various amino acids, in particular branched-chain amino acids (BCAA), were more abundant when U was applied (**Figure S7**). An increase in BCAA biosynthesis could be explained by their important role in plant responses to a wide range of abiotic stresses [73], including cadmium stress [74,75]. In this context, the accumulation of Leu, Ile and Val may serve to promote stress-induced protein synthesis [76]. The accumulation of several aminoacyl tRNA ligases in response to U stress supports this hypothesis (**Figure S7**). The accumulation of enzymes involved in BCAA biosynthesis may

546 also reflect a compensatory mechanism due to their rapid catabolism to cope with U stress. In fact, the
547 breakdown products of BCAAs (*e.g.* acetyl-CoA, propionyl-CoA, acetoacetate) are potential energy
548 sources for plants [77]. Besides, the biosynthetic pathway of aromatic amino acids was also increased
549 in response to U stress (**Figure S7**). In this case, Trp could serve for the biosynthesis of phytohormones
550 (*i.e*. auxin) whereas Phe could be required for the phenylpropanoid pathway to produce a wide range of
551 plant secondary products, especially antioxidative metabolites (flavonoids, anthocyanins, lignins) and
552 phenolic compounds in response to abiotic stress such as U.
553
554 **4.3. Identification of transport and endomembrane trafficking processes potentially involved in**
555 **U distribution and sequestration**
556 Regarding U trafficking in plants, only the contribution of the calcium channels ANN1 and MCA1 to root
557 U uptake has been experimentally demonstrated [22]. The identification of transporters involved in
558 intracellular U trafficking remains to be elucidated, with only a few clues available from gene expression
559 analysis of plants challenged with U [8,13,25]. Our proteomic approach points out the differential
560 accumulation of several transporters belonging to the ABC transporter family (**Figure 6D**). This
561 transporter family has been shown to fulfill highly divergent physiological functions, including heavy
562 metal tolerance in plants [78]. The phytochelatin transporter ABCC2 may be relevant for U detoxification,
563 as this protein confers tolerance to several heavy metals, including arsenic, cadmium, and mercury
564 [79,80]. The ABCB1 and ABCB11 auxin transporters may also play a significant indirect role in U
565 tolerance. ABCB11 may be of particular interest as it is highly active in roots and auxin transport is
566 impaired in the corresponding Arabidopsis mutant [81,82]. The down accumulation of ABCB11 is
567 consistent with the disrupted transport and gradient of auxin observed in the root apex under U stress
568 [16]. Zinc, copper, cadmium or uncharacterized transport proteins are also deregulated by high U
569 concentrations (**Figure 6D**). Together with ABC transporters, these proteins may represent relevant
570 molecular actors in U tolerance, either by maintaining the homeostasis of essential metals or by
571 modulating hormonal transport.
572 This analysis also revealed the importance of endomembrane trafficking in the response of plants to U
573 stress. More specifically, proteins involved in trafficking between the ER and Golgi apparatus, in pre-
574 vacuolar compartments/multi vesicular body formation (*i.e.* ESCRT complexes), and in the secretory
575 pathway were significantly deregulated upon U stress (**Figure 6C; Figure S8**). The involvement of
576 endocytosis in U uptake has been recently proposed in tobacco cells [26]. Here, a hypothetical scenario
577 would be that uranyl ions, U target proteins or other proteins contributing to U toxicity are internalized
578 into vesicles before being released towards the apoplast or stored/degraded in the vacuole.
579
580 **4.4. Uranium alters cell wall dynamics by regulating pectin modifications and Casparian strip**
581 **formation**

582 Previous studies have shown that a high proportion of uranyl ions in plant roots are associated with the
583 cell wall, which is rich in negatively charged groups with a high affinity for metal cations [8–10]. Our
584 analysis supports important changes in cell wall composition in response to U stress, including lignin
585 and suberin synthesis, pectin modification, polysaccharide hydrolysis, and Casparian strips formation
586 (**Figure 6B**). The abundance of three pectin methylesterases and one acetylesterase was decreased
587 during U stress (**Figure 6B**). A negative relationship between the degree of methylesterification and
588 acetylation of pectins, and their ability to bind some heavy metals (*i.e.* aluminum, lead, copper), has
589 been reported in plants [83–85]. By maintaining a high degree of pectin esterification, plants could
590 improve their tolerance to U by limiting heavy metal accumulation in their tissues, thus preventing
591 transport to intracellular compartments. Another adaptive strategy in response to heavy metal
592 intoxication could involve structural changes in roots. In fact, our analysis shows that the CASP protein
593 family and the UCC2 protein, which are involved in the formation of lignin-based Casparian strips in the
594 root endodermis [60–62], are down-accumulated during U stress (**Figure 6B**). Thus, a strong defect in
595 root apoplastic permeability caused by a disruption of Casparian strips would facilitate the radial transfer
596 of U in roots, and ultimately its translocation toward aboveground organs. This is obviously not the case,
597 as we observed a very low accumulation of U in the shoots of treated plants (**Figure S1**). Instead, the
598 limitation in U translocation from roots to shoots would rather induce a U-dependent ectopic callose
599 deposition. This is accompanied by an enhanced suberization, caused by a reduction in the abundance
600 of CASP and UCC2 proteins, similar to what is observed in the corresponding Arabidopsis loss-of-
601 function mutants [61,62]. Reinforcing this hypothesis, several enzymes involved in suberin synthesis
602 are up-accumulated during U stress (**Figure 6B**). Also, the deposition of callose and lignin in lateral
603 roots, together with structural damage to root epidermal cells, have already been observed in response
604 to U in Arabidopsis and *V. faba* [8,16].
605
606 **4.5. Uranium affects plant water balance through an aquaporin-driven disruption**
607 We showed that eight aquaporins were down-accumulated in the roots of Arabidopsis plants stressed
608 by U (**Figure 6D**), including PIP1;2 and PIP2;1, the two major contributors for water transport in
609 Arabidopsis roots [86,87]. Corroborating these results, a significant reduction in aquaporin-related root
610 hydraulic conductivity and leaf transpiration were measured in response to U stress (**Figure 8**). One
611 hypothesis is that the decrease in aquaporin levels serves as a protective mechanism to limit U
612 accumulation in roots, due to the permeability of aquaporins to U. Indeed, an aquaporin-mediated
613 transport of metalloids has been reported in plants. This is particularly the case for nodulin 26-like
614 intrinsic protein 1.1 (NIP1.1), which has been shown to transport antimony and arsenite in Arabidopsis
615 [88,89]. However, we found no evidence that U affects the abundance of NIP proteins, and the transport
616 of any metal by PIP aquaporins remains to be demonstrated. Alternatively, a decrease in aquaporin
617 levels, and the resulting reduced whole plant water flow, could act as a mechanism to limit the solvent-

drag of U. This reduction would decrease U uptake and relocation to shoots, thereby limiting its harmful effects. This hypothesis is attractive because water transport has been shown to be an important process regulating the partitioning and accumulation of U [70].

The mechanism by which U modifies the abundance of aquaporins in Arabidopsis roots remains to be determined. Several direct or indirect scenarios can be considered (**Figure S9**). First, U could regulate the steady-state level of aquaporins via transcriptional regulation. The differential expression of aquaporin encoding genes under different heavy metal stress conditions (*e.g.* cadmium, arsenic, zinc and boron) has been observed in various plant species (see [90] for a review; [91]). However, transcriptional regulation of *PIP* genes seems unlikely in Arabidopsis under U stress as *PIP* transcript levels are unchanged in roots and only slightly modified in leaves in these conditions [13,70]. Second, U might regulate PIP aquaporins at the post-translational level, in particular through modifications affecting their stability and turnover. Noteworthy, some PIPs are ubiquitinated in a process that is dependent on the E2 ubiquitin-conjugating enzyme UBC32, a component of the ER-associated degradation (ERAD) pathway, and the RING-type E3 ligase Rma1 [92,93]. Genes coding some components of the ERAD pathway, including several E3 ubiquitin-protein ligases, were found upregulated in the roots of *Raphanus sativus* plants challenged with U [10]. Also, we found that the abundance of two ubiquitin-conjugating enzymes (UBC7 and UEV1D) is increased in Arabidopsis root during U50 stress (**Table S5**). Together, these data support the hypothesis that a U-dependent ubiquitination of PIP aquaporins could promote their degradation, thereby enhancing stress tolerance, as show for drought stress [93,94]. Third, U might indirectly cause a decrease in aquaporin protein levels by compromising the integrity of root endodermal barriers. Indeed, several studies using Casparian strip and suberin deficient Arabidopsis mutants have shown that activation of the CIF1&2/SCHENGEN3 (CIFs/SGN3) surveillance pathway triggers the ectopic deposition of suberin and lignin in roots. This process is associated with the deactivation of aquaporin activity through an unclear mechanism (see details in **Figure S9** caption) [95–98]. Such a regulatory process is plausible as U stress leads to a decrease in aquaporins and CASP proteins abundance (**Figure 6BD**), an accumulation of some lignin and suberin synthesizing proteins (**Figure 6B**), and a reduction in root hydraulics and leaf transpiration (**Figure 8**). Also, extra-lignification was observed in Arabidopsis roots under U stress [16]. Further investigations are needed to confirm or refute these hypotheses.

5 - Conclusion

To conclude, our results show that Arabidopsis roots orchestrate an important rearrangement of the cell wall and membrane proteome in response to U stress. Our proteomic data provide insights into the biological processes disrupted by U in this fraction of the global proteome, thereby enhancing our understanding of the mechanisms by which plants cope with metal toxicity. To validate some of these mechanisms, functional analysis showed that a preventive mechanism to limit the harmful effects of U

is a reduction of water flow in roots through the repression of aquaporins and CASP proteins, together with modifications of the synthesis and deposition of cell wall polymers. This study also identifies transporters and metal-binding proteins that may be involved in the fate of U in Arabidopsis. Further functional studies are needed to clarify the contribution of these proteins to U tolerance.

Declaration of Competing Interest

The authors declare that they have no known competing financial interests or personal relationships that could have appeared to influence the work reported in this paper.

Funding resources

This work was funded by the Agence Nationale de la Recherche (ANR-17-CE34-0007, GreenU and ANR-17-EURE-0003, CBH-EUR-GS).

References

[1] M. Anke, O. Seeber, R. Müller, U. Schäfer, J. Zerull, Uranium transfer in the food chain from soil to plants, animals and man, Geochemistry 69 (2009) 75–90. https://doi.org/10.1016/j.chemer.2007.12.001.

[2] L. Chen, J. Liu, W. Zhang, J. Zhou, D. Luo, Z. Li, Uranium (U) source, speciation, uptake, toxicity and bioremediation strategies in soil-plant system: A review, Journal of Hazardous Materials 413 (2021) 125319. https://doi.org/10.1016/j.jhazmat.2021.125319.

[3] O. Neves, M.M. Abreu, Are uranium-contaminated soil and irrigation water a risk for human vegetables consumers? A study case with Solanum tuberosum L., Phaseolus vulgaris L. and Lactuca sativa L, Ecotoxicology 18 (2009) 1130–1136. https://doi.org/10.1007/s10646-009-0376-4.

[4] A. Martin, Y. Hassan-Loni, A. Fichtner, O. Péron, K. David, P. Chardon, S. Larrue, A. Gourgiotis, S. Sachs, T. Arnold, B. Grambow, T. Stumpf, G. Montavon, An integrated approach combining soil profile, records and tree ring analysis to identify the origin of environmental contamination in a former uranium mine (Rophin, France), Sci Total Environ 747 (2020) 141295. https://doi.org/10.1016/j.scitotenv.2020.141295.

[5] M.O. Neves, M.M. Abreu, V. Figueiredo, Uranium in vegetable foodstuffs: should residents near the Cunha Baixa uranium mine site (Central Northern Portugal) be concerned?, Environ Geochem Health 34 (2012) 181–189. https://doi.org/10.1007/s10653-011-9428-9.

[6] H. Vandenhove, European sites contaminated by residues from the ore-extracting and -processing industries, International Congress Series 1225 (2002) 307–315. https://doi.org/10.1016/S0531-5131(01)00525-8.

[7] J. Hu, Z. Wang, G.D.Z. Williams, G.S. Dwyer, L. Gatiboni, O.W. Duckworth, A. Vengosh, Evidence for the accumulation of toxic metal(loid)s in agricultural soils impacted from long-term application of phosphate fertilizer, Science of The Total Environment 907 (2024) 167863. https://doi.org/10.1016/j.scitotenv.2023.167863.

[8] J. Lai, Z. Liu, X. Luo, A metabolomic, transcriptomic profiling, and mineral nutrient metabolism study of the phytotoxicity mechanism of uranium, Journal of Hazardous Materials 386 (2020) 121437. https://doi.org/10.1016/j.jhazmat.2019.121437.

[9] M.C.M. Sarthou, B.H. Revel, F. Villiers, C. Alban, T. Bonnot, O. Gigarel, A.-M. Boisson, S. Ravanel, J. Bourguignon, Development of a metalloproteomic approach to analyse the response of Arabidopsis cells to uranium stress, Metallomics 12 (2020) 1302–1313. https://doi.org/10.1039/d0mt00092b.

[10] X. Chen, Y. Dang, Q. Li, W. Li, M. Xie, M. Wang, M. Tao, S. Zhao, J. Lai, G. Wu, Uranium affects nitrogen metabolism and endoplasmic reticulum protein homeostasis in plants, Environmental and Experimental Botany 213 (2023) 105444. https://doi.org/10.1016/j.envexpbot.2023.105444.

[11] N. Vanhoudt, H. Vandenhove, N. Horemans, J. Wannijn, M. Van Hees, J. Vangronsveld, A. Cuypers, The combined effect of uranium and gamma radiation on biological responses and oxidative stress induced in Arabidopsis thaliana, J Environ Radioact 101 (2010) 923–930. https://doi.org/10.1016/j.jenvrad.2010.06.008.

[12] N. Vanhoudt, H. Vandenhove, N. Horemans, D. Martinez Bello, M. Van Hees, J. Wannijn, R. Carleer, J. Vangronsveld, A. Cuypers, Uranium Induced Effects on Development and Mineral Nutrition of Arabidopsis Thaliana, Journal of Plant Nutrition 34 (2011) 1940–1956. https://doi.org/10.1080/01904167.2011.610482.

[13] F. Doustaly, F. Combes, J.B. Fiévet, S. Berthet, V. Hugouvieux, O. Bastien, I. Aranjuelo, N. Leonhardt, C. Rivasseau, M. Carrière, A. Vavasseur, J.-P. Renou, Y. Vandenbrouck, J. Bourguignon, Uranium perturbs signaling and iron uptake response in Arabidopsis thaliana roots, Metallomics 6 (2014) 809–821. https://doi.org/10.1039/c4mt00005f.

[14] E. Saenen, N. Horemans, N. Vanhoudt, H. Vandenhove, G. Biermans, M. Van Hees, J. Wannijn, J. Vangronsveld, A. Cuypers, The pH strongly influences the uranium-induced effects on the photosynthetic apparatus of Arabidopsis thaliana plants, Plant Physiol Biochem 82 (2014) 254–261. https://doi.org/10.1016/j.plaphy.2014.06.012.

[15] E. Saenen, N. Horemans, N. Vanhoudt, H. Vandenhove, G. Biermans, M. Van Hees, J. Wannijn, J. Vangronsveld, A. Cuypers, Induction of Oxidative Stress and Antioxidative Mechanisms in

Arabidopsis thaliana after Uranium Exposure at pH 7.5, Int J Mol Sci 16 (2015) 12405–12423. https://doi.org/10.3390/ijms160612405.
[16] N.B.C. Serre, C. Alban, J. Bourguignon, S. Ravanel, Uncovering the physiological and cellular effects of uranium on the root system of Arabidopsis thaliana, Environmental and Experimental Botany 157 (2019) 121–130. https://doi.org/10.1016/j.envexpbot.2018.10.004.
[17] G. Wu, X. Chen, T. Zheng, P. Xiao, N. Zhong, X. Yang, Y. Li, W. Li, Effects of U on the growth, reactive oxygen metabolism and osmotic regulation in radish (Raphanus sativus L.), Environ Sci Pollut Res 29 (2022) 55081–55091. https://doi.org/10.1007/s11356-022-19803-w.
[18] X. Chen, G. Wu, P. Xiao, Q. Ma, Y. Li, J. Lai, X. Luo, X. Ji, J. Xia, X. Yang, A new perspective on the inhibition of plant photosynthesis by uranium: decrease of root activity and stomatal closure, Int J Phytoremediation 24 (2022) 1071–1080. https://doi.org/10.1080/15226514.2021.2002260.
[19] D.K. Gupta, A. Vuković, V.S. Semenishchev, M. Inouhe, C. Walther, Uranium accumulation and its phytotoxicity symptoms in Pisum sativum L., Environ Sci Pollut Res 27 (2020) 3513–3522. https://doi.org/10.1007/s11356-019-07068-9.
[20] P.-X. Xiao, X. Chen, N.-Y. Zhong, T. Zheng, Y.-M. Wang, G. Wu, H. Zhang, B. He, Response of Vicia faba to short-term uranium exposure: chelating and antioxidant system changes in roots, J Plant Res 136 (2023) 413–421. https://doi.org/10.1007/s10265-023-01443-x.
[21] F. Rajabi, J. Jessat, J.N. Garimella, F. Bok, R. Steudtner, T. Stumpf, S. Sachs, Uranium(VI) toxicity in tobacco BY-2 cell suspension culture – A physiological study, Ecotoxicology and Environmental Safety 211 (2021) 111883. https://doi.org/10.1016/j.ecoenv.2020.111883.
[22] M.C.M. Sarthou, F. Devime, C. Baggio, S. Figuet, C. Alban, J. Bourguignon, S. Ravanel, Calcium-permeable cation channels are involved in uranium uptake in Arabidopsis thaliana, J Hazard Mater 424 (2022) 127436. https://doi.org/10.1016/j.jhazmat.2021.127436.
[23] S. Berthet, F. Villiers, C. Alban, N.B.C. Serre, J. Martin-Laffon, S. Figuet, A.-M. Boisson, R. Bligny, M. Kuntz, G. Finazzi, S. Ravanel, J. Bourguignon, Arabidopsis thaliana plants challenged with uranium reveal new insights into iron and phosphate homeostasis, New Phytol 217 (2018) 657–670. https://doi.org/10.1111/nph.14865.
[24] B. Revel, P. Catty, S. Ravanel, J. Bourguignon, C. Alban, High-affinity iron and calcium transport pathways are involved in U(VI) uptake in the budding yeast Saccharomyces cerevisiae, J Hazard Mater 422 (2022) 126894. https://doi.org/10.1016/j.jhazmat.2021.126894.
[25] A. Mertens, N. Horemans, E. Saenen, R. Nauts, A. Cuypers, Calcium affects uranium responses in Arabidopsis thaliana: From distribution to toxicity, Plant Physiology and Biochemistry 185 (2022) 101–111. https://doi.org/10.1016/j.plaphy.2022.05.020.
[26] W.A. John, B. Lückel, N. Matschiavelli, R. Hübner, S. Matschi, W. Hoehenwarter, S. Sachs, Endocytosis is a significant contributor to uranium(VI) uptake in tobacco (Nicotiana tabacum) BY-2 cells in phosphate-deficient culture, Sci Total Environ 823 (2022) 153700. https://doi.org/10.1016/j.scitotenv.2022.153700.
[27] Y. Zhang, J.-L. Lai, X.-H. Ji, X.-G. Luo, Unraveling response mechanism of photosynthetic metabolism and respiratory metabolism to uranium-exposure in Vicia faba, J Hazard Mater 398 (2020) 122997. https://doi.org/10.1016/j.jhazmat.2020.122997.
[28] J.-L. Lai, Z.-W. Liu, C. Li, X.-G. Luo, Analysis of accumulation and phytotoxicity mechanism of uranium and cadmium in two sweet potato cultivars, J Hazard Mater 409 (2021) 124997. https://doi.org/10.1016/j.jhazmat.2020.124997.
[29] A. Vallet, J. Martin-Laffon, A. Favier, B. Revel, T. Bonnot, C. Vidaud, J. Armengaud, J.-C. Gaillard, P. Delangle, F. Devime, S. Figuet, N.B.C. Serre, E.B. Erba, B. Brutscher, S. Ravanel, J. Bourguignon, C. Alban, The plasma membrane-associated cation-binding protein PCaP1 of Arabidopsis thaliana is a uranyl-binding protein, J Hazard Mater 446 (2023) 130668. https://doi.org/10.1016/j.jhazmat.2022.130668.
[30] N. Nagasaki, R. Tomioka, M. Maeshima, A hydrophilic cation-binding protein of Arabidopsis thaliana, AtPCaP1, is localized to plasma membrane via N-myristoylation and interacts with calmodulin and the phosphatidylinositol phosphates PtdIns(3,4,5)P(3) and PtdIns(3,5)P(2), FEBS J 275 (2008) 2267–2282. https://doi.org/10.1111/j.1742-4658.2008.06379.x.
[31] J. Li, X. Wang, T. Qin, Y. Zhang, X. Liu, J. Sun, Y. Zhou, L. Zhu, Z. Zhang, M. Yuan, T. Mao, MDP25,

a novel calcium regulatory protein, mediates hypocotyl cell elongation by destabilizing cortical microtubules in Arabidopsis, Plant Cell 23 (2011) 4411–4427. https://doi.org/10.1105/tpc.111.092684.
[32] N. Gallois, B. Alpha-Bazin, N. Bremond, P. Ortet, M. Barakat, L. Piette, A. Mohamad Ali, D. Lemaire, P. Legrand, N. Theodorakopoulos, M. Floriani, L. Février, C. Den Auwer, P. Arnoux, C. Berthomieu, J. Armengaud, V. Chapon, Discovery and characterization of UipA, a uranium- and iron-binding PepSY protein involved in uranium tolerance by soil bacteria, ISME J 16 (2022) 705–716. https://doi.org/10.1038/s41396-021-01113-7.
[33] M. Mininno, S. Brugière, V. Pautre, A. Gilgen, S. Ma, M. Ferro, M. Tardif, C. Alban, S. Ravanel, Characterization of chloroplastic fructose 1,6-bisphosphate aldolases as lysine-methylated proteins in plants, J Biol Chem 287 (2012) 21034–21044. https://doi.org/10.1074/jbc.M112.359976.
[34] B. Revel, Identification de protéines impliquées dans le devenir de l'uranium dans la plante Arabidopsis thaliana et la levure Saccharomyces cerevisiae., These de doctorat, Université Grenoble Alpes, 2021. https://theses.fr/2021GRALV004 (accessed August 24, 2024).
[35] D. Kessner, M. Chambers, R. Burke, D. Agus, P. Mallick, ProteoWizard: open source software for rapid proteomics tools development, Bioinformatics 24 (2008) 2534–2536. https://doi.org/10.1093/bioinformatics/btn323.
[36] R. Craig, R.C. Beavis, TANDEM: matching proteins with tandem mass spectra, Bioinformatics 20 (2004) 1466–1467. https://doi.org/10.1093/bioinformatics/bth092.
[37] O. Langella, B. Valot, T. Balliau, M. Blein-Nicolas, L. Bonhomme, M. Zivy, X!TandemPipeline: A Tool to Manage Sequence Redundancy for Protein Inference and Phosphosite Identification, J Proteome Res 16 (2017) 494–503. https://doi.org/10.1021/acs.jproteome.6b00632.
[38] B. Valot, O. Langella, E. Nano, M. Zivy, MassChroQ: a versatile tool for mass spectrometry quantification, Proteomics 11 (2011) 3572–3577. https://doi.org/10.1002/pmic.201100120.
[39] A. Kowarik, M. Templ, Imputation with the R Package VIM, Journal of Statistical Software 74 (2016) 1–16. https://doi.org/10.18637/jss.v074.i07.
[40] J. Herrero, A. Valencia, J. Dopazo, A hierarchical unsupervised growing neural network for clustering gene expression patterns, Bioinformatics 17 (2001) 126–136. https://doi.org/10.1093/bioinformatics/17.2.126.
[41] C.M. Hooper, I.R. Castleden, S.K. Tanz, N. Aryamanesh, A.H. Millar, SUBA4: the interactive data analysis centre for Arabidopsis subcellular protein locations, Nucleic Acids Res 45 (2017) D1064–D1074. https://doi.org/10.1093/nar/gkw1041.
[42] S. Babicki, D. Arndt, A. Marcu, Y. Liang, J.R. Grant, A. Maciejewski, D.S. Wishart, Heatmapper: web-enabled heat mapping for all, Nucleic Acids Res 44 (2016) W147-153. https://doi.org/10.1093/nar/gkw419.
[43] S. Maere, K. Heymans, M. Kuiper, BiNGO: a Cytoscape plugin to assess overrepresentation of gene ontology categories in biological networks, Bioinformatics 21 (2005) 3448–3449. https://doi.org/10.1093/bioinformatics/bti551.
[44] Y. Zhou, B. Zhou, L. Pache, M. Chang, A.H. Khodabakhshi, O. Tanaseichuk, C. Benner, S.K. Chanda, Metascape provides a biologist-oriented resource for the analysis of systems-level datasets, Nat Commun 10 (2019) 1523. https://doi.org/10.1038/s41467-019-09234-6.
[45] P. Gloaguen, Y. Vandenbrouck, J. Joyard, G. Curien, ChloroKB, a cell metabolism reconstruction of the model plant Arabidopsis thaliana, C R Biol 344 (2021) 157–163. https://doi.org/10.5802/crbiol.49.
[46] Y. Boursiac, S. Chen, D.-T. Luu, M. Sorieul, N. van den Dries, C. Maurel, Early effects of salinity on water transport in Arabidopsis roots. Molecular and cellular features of aquaporin expression, Plant Physiol 139 (2005) 790–805. https://doi.org/10.1104/pp.105.065029.
[47] J. Misson, P. Henner, M. Morello, M. Floriani, T.-D. Wu, J.-L. Guerquin-Kern, L. Février, Use of phosphate to avoid uranium toxicity in Arabidopsis thaliana leads to alterations of morphological and physiological responses regulated by phosphate availability, Environmental and Experimental Botany 67 (2009) 353–362. https://doi.org/10.1016/j.envexpbot.2009.09.001.
[48] J. Laurette, C. Larue, C. Mariet, F. Brisset, H. Khodja, J. Bourguignon, M. Carrière, Influence of uranium speciation on its accumulation and translocation in three plant species: Oilseed rape,

sunflower and wheat, Environmental and Experimental Botany 77 (2012) 96–107. https://doi.org/10.1016/j.envexpbot.2011.11.007.
[49] J.H. Kim, N.H. Nguyen, N.T. Nguyen, S.-W. Hong, H. Lee, Loss of all three calreticulins, CRT1, CRT2 and CRT3, causes enhanced sensitivity to water stress in Arabidopsis, Plant Cell Rep 32 (2013) 1843–1853. https://doi.org/10.1007/s00299-013-1497-z.
[50] J. Maszkowska, J. Dębski, A. Kulik, M. Kistowski, M. Bucholc, M. Lichocka, M. Klimecka, O. Sztatelman, K.P. Szymańska, M. Dadlez, G. Dobrowolska, Phosphoproteomic analysis reveals that dehydrins ERD10 and ERD14 are phosphorylated by SNF1-related protein kinase 2.10 in response to osmotic stress, Plant Cell Environ 42 (2019) 931–946. https://doi.org/10.1111/pce.13465.
[51] G. Merkouropoulos, E. Andreasson, D. Hess, T. Boller, S.C. Peck, An Arabidopsis protein phosphorylated in response to microbial elicitation, AtPHOS32, is a substrate of MAP kinases 3 and 6, J Biol Chem 283 (2008) 10493–10499. https://doi.org/10.1074/jbc.M800735200.
[52] J.-E. Sarry, L. Kuhn, C. Ducruix, A. Lafaye, C. Junot, V. Hugouvieux, A. Jourdain, O. Bastien, J.B. Fievet, D. Vailhen, B. Amekraz, C. Moulin, E. Ezan, J. Garin, J. Bourguignon, The early responses of Arabidopsis thaliana cells to cadmium exposure explored by protein and metabolite profiling analyses, Proteomics 6 (2006) 2180–2198. https://doi.org/10.1002/pmic.200500543.
[53] Y. Fukao, A. Ferjani, M. Fujiwara, Y. Nishimori, I. Ohtsu, Identification of zinc-responsive proteins in the roots of Arabidopsis thaliana using a highly improved method of two-dimensional electrophoresis, Plant Cell Physiol 50 (2009) 2234–2239. https://doi.org/10.1093/pcp/pcp154.
[54] F. Gaymard, J. Boucherez, J.F. Briat, Characterization of a ferritin mRNA from Arabidopsis thaliana accumulated in response to iron through an oxidative pathway independent of abscisic acid, Biochem J 318 (Pt 1) (1996) 67–73. https://doi.org/10.1042/bj3180067.
[55] N. Nagasaki-Takeuchi, M. Miyano, M. Maeshima, A plasma membrane-associated protein of Arabidopsis thaliana AtPCaP1 binds copper ions and changes its higher order structure, J Biochem 144 (2008) 487–497. https://doi.org/10.1093/jb/mvn092.
[56] S. Harun, M.-R. Abdullah-Zawawi, H.-H. Goh, Z.-A. Mohamed-Hussein, A Comprehensive Gene Inventory for Glucosinolate Biosynthetic Pathway in Arabidopsis thaliana, J. Agric. Food Chem. 68 (2020) 7281–7297. https://doi.org/10.1021/acs.jafc.0c01916.
[57] C.M. Fraser, C. Chapple, The phenylpropanoid pathway in Arabidopsis, Arabidopsis Book 9 (2011) e0152. https://doi.org/10.1199/tab.0152.
[58] O. Serra, N. Geldner, The making of suberin, New Phytol 235 (2022) 848–866. https://doi.org/10.1111/nph.18202.
[59] Z. Minic, L. Jouanin, Plant glycoside hydrolases involved in cell wall polysaccharide degradation, Plant Physiol Biochem 44 (2006) 435–449. https://doi.org/10.1016/j.plaphy.2006.08.001.
[60] D. Roppolo, B. De Rybel, V. Dénervaud Tendon, A. Pfister, J. Alassimone, J.E.M. Vermeer, M. Yamazaki, Y.-D. Stierhof, T. Beeckman, N. Geldner, A novel protein family mediates Casparian strip formation in the endodermis, Nature 473 (2011) 380–383. https://doi.org/10.1038/nature10070.
[61] G. Reyt, Z. Chao, P. Flis, I. Salas-González, G. Castrillo, D.-Y. Chao, D.E. Salt, Uclacyanin Proteins Are Required for Lignified Nanodomain Formation within Casparian Strips, Curr Biol 30 (2020) 4103-4111.e6. https://doi.org/10.1016/j.cub.2020.07.095.
[62] I.C.R. Barbosa, D. De Bellis, I. Flückiger, E. Bellani, M. Grangé-Guerment, K. Hématy, N. Geldner, Directed growth and fusion of membrane-wall microdomains requires CASP-mediated inhibition and displacement of secretory foci, Nat Commun 14 (2023) 1626. https://doi.org/10.1038/s41467-023-37265-7.
[63] C. Gao, X. Zhuang, J. Shen, L. Jiang, Plant ESCRT Complexes: Moving Beyond Endosomal Sorting, Trends in Plant Science 22 (2017) 986–998. https://doi.org/10.1016/j.tplants.2017.08.003.
[64] C. Tournaire-Roux, M. Sutka, H. Javot, E. Gout, P. Gerbeau, D.-T. Luu, R. Bligny, C. Maurel, Cytosolic pH regulates root water transport during anoxic stress through gating of aquaporins, Nature 425 (2003) 393–397. https://doi.org/10.1038/nature01853.
[65] M. Sutka, G. Li, J. Boudet, Y. Boursiac, P. Doumas, C. Maurel, Natural variation of root hydraulics in Arabidopsis grown in normal and salt-stressed conditions, Plant Physiol 155 (2011) 1264–1276. https://doi.org/10.1104/pp.110.163113.
[66] S.A. Ghuge, G.C. Nikalje, U.S. Kadam, P. Suprasanna, J.C. Hong, Comprehensive mechanisms of

heavy metal toxicity in plants, detoxification, and remediation, J Hazard Mater 450 (2023) 131039. https://doi.org/10.1016/j.jhazmat.2023.131039.
[67] K.J. Waldron, J.C. Rutherford, D. Ford, N.J. Robinson, Metalloproteins and metal sensing, Nature 460 (2009) 823–830. https://doi.org/10.1038/nature08300.
[68] C. Vidaud, S. Gourion-Arsiquaud, F. Rollin-Genetet, C. Torne-Celer, S. Plantevin, O. Pible, C. Berthomieu, E. Quéméneur, Structural consequences of binding of UO2(2+) to apotransferrin: can this protein account for entry of uranium into human cells?, Biochemistry 46 (2007) 2215–2226. https://doi.org/10.1021/bi061945h.
[69] R. Pardoux, S. Sauge-Merle, D. Lemaire, P. Delangle, L. Guilloreau, J.-M. Adriano, C. Berthomieu, Modulating uranium binding affinity in engineered calmodulin EF-hand peptides: effect of phosphorylation, PLoS One 7 (2012) e41922. https://doi.org/10.1371/journal.pone.0041922.
[70] I. Aranjuelo, F. Doustaly, J. Cela, R. Porcel, M. Müller, R. Aroca, S. Munné-Bosch, J. Bourguignon, Glutathione and transpiration as key factors conditioning oxidative stress in Arabidopsis thaliana exposed to uranium, Planta 239 (2014) 817–830. https://doi.org/10.1007/s00425-013-2014-x.
[71] R. Tewari, N. Horemans, R. Nauts, J. Wannijn, M. Van Hees, H. Vandenhove, Uranium exposure induces nitric oxide and hydrogen peroxide generation in Arabidopsis thaliana, Environmental and Experimental Botany 120 (2015) 55–64. https://doi.org/10.1016/j.envexpbot.2015.08.004.
[72] Y. Zhang, A.R. Fernie, Metabolons, enzyme-enzyme assemblies that mediate substrate channeling, and their roles in plant metabolism, Plant Commun 2 (2021) 100081. https://doi.org/10.1016/j.xplc.2020.100081.
[73] T. Obata, A.R. Fernie, The use of metabolomics to dissect plant responses to abiotic stresses, Cell Mol Life Sci 69 (2012) 3225–3243. https://doi.org/10.1007/s00018-012-1091-5.
[74] V. Zemanová, M. Pavlík, D. Pavlíková, Cadmium toxicity induced contrasting patterns of concentrations of free sarcosine, specific amino acids and selected microelements in two Noccaea species, PLoS One 12 (2017) e0177963. https://doi.org/10.1371/journal.pone.0177963.
[75] Y. Zhao, C. Zhang, C. Wang, Y. Huang, Z. Liu, Increasing phosphate inhibits cadmium uptake in plants and promotes synthesis of amino acids in grains of rice, Environmental Pollution 257 (2020) 113496. https://doi.org/10.1016/j.envpol.2019.113496.
[76] E. Nambara, H. Kawaide, Y. Kamiya, S. Naito, Characterization of an Arabidopsis thaliana mutant that has a defect in ABA accumulation: ABA-dependent and ABA-independent accumulation of free amino acids during dehydration, Plant Cell Physiol 39 (1998) 853–858. https://doi.org/10.1093/oxfordjournals.pcp.a029444.
[77] V. Joshi, J.-G. Joung, Z. Fei, G. Jander, Interdependence of threonine, methionine and isoleucine metabolism in plants: accumulation and transcriptional regulation under abiotic stress, Amino Acids 39 (2010) 933–947. https://doi.org/10.1007/s00726-010-0505-7.
[78] W.-Y. Song, J. Park, C. Eisenach, M. Maeshima, Y. Lee, E. Martinoia, ABC Transporters and Heavy Metals, in: M. Geisler (Ed.), Plant ABC Transporters, Springer International Publishing, Cham, 2014: pp. 1–17. https://doi.org/10.1007/978-3-319-06511-3_1.
[79] W.-Y. Song, J. Park, D.G. Mendoza-Cózatl, M. Suter-Grotemeyer, D. Shim, S. Hörtensteiner, M. Geisler, B. Weder, P.A. Rea, D. Rentsch, J.I. Schroeder, Y. Lee, E. Martinoia, Arsenic tolerance in Arabidopsis is mediated by two ABCC-type phytochelatin transporters, Proceedings of the National Academy of Sciences 107 (2010) 21187–21192. https://doi.org/10.1073/pnas.1013964107.
[80] J. Park, W.-Y. Song, D. Ko, Y. Eom, T.H. Hansen, M. Schiller, T.G. Lee, E. Martinoia, Y. Lee, The phytochelatin transporters AtABCC1 and AtABCC2 mediate tolerance to cadmium and mercury, Plant J 69 (2012) 278–288. https://doi.org/10.1111/j.1365-313X.2011.04789.x.
[81] M. Kaneda, M. Schuetz, B.S.P. Lin, C. Chanis, B. Hamberger, T.L. Western, J. Ehlting, A.L. Samuels, ABC transporters coordinately expressed during lignification of Arabidopsis stems include a set of ABCBs associated with auxin transport, J Exp Bot 62 (2011) 2063–2077. https://doi.org/10.1093/jxb/erq416.
[82] M.K. Jenness, R. Tayengwa, G.A. Bate, W. Tapken, Y. Zhang, C. Pang, A.S. Murphy, Loss of Multiple ABCB Auxin Transporters Recapitulates the Major twisted dwarf 1 Phenotypes in Arabidopsis thaliana, Front. Plant Sci. 13 (2022). https://doi.org/10.3389/fpls.2022.840260.
[83] M. Khotimchenko, V. Kovalev, Y. Khotimchenko, Equilibrium studies of sorption of lead(II) ions by

different pectin compounds, J Hazard Mater 149 (2007) 693–699. https://doi.org/10.1016/j.jhazmat.2007.04.030.
[84] T. Mimmo, C. Marzadori, C.E. Gessa, Does the degree of pectin esterification influence aluminium sorption by the root apoplast?, Plant Soil 314 (2009) 159–168. https://doi.org/10.1007/s11104-008-9715-0.
[85] I. Colzi, M. Arnetoli, A. Gallo, S. Doumett, M. Del Bubba, S. Pignattelli, R. Gabbrielli, C. Gonnelli, Copper tolerance strategies involving the root cell wall pectins in Silene paradoxa L., Environmental and Experimental Botany 78 (2012) 91–98. https://doi.org/10.1016/j.envexpbot.2011.12.028.
[86] O. Postaire, C. Tournaire-Roux, A. Grondin, Y. Boursiac, R. Morillon, A.R. Schäffner, C. Maurel, A PIP1 aquaporin contributes to hydrostatic pressure-induced water transport in both the root and rosette of Arabidopsis, Plant Physiol 152 (2010) 1418–1430. https://doi.org/10.1104/pp.109.145326.
[87] B. Péret, G. Li, J. Zhao, L.R. Band, U. Voß, O. Postaire, D.-T. Luu, O. Da Ines, I. Casimiro, M. Lucas, D.M. Wells, L. Lazzerini, P. Nacry, J.R. King, O.E. Jensen, A.R. Schäffner, C. Maurel, M.J. Bennett, Auxin regulates aquaporin function to facilitate lateral root emergence, Nat Cell Biol 14 (2012) 991–998. https://doi.org/10.1038/ncb2573.
[88] T. Kamiya, M. Tanaka, N. Mitani, J.F. Ma, M. Maeshima, T. Fujiwara, NIP1;1, an aquaporin homolog, determines the arsenite sensitivity of Arabidopsis thaliana, J Biol Chem 284 (2009) 2114–2120. https://doi.org/10.1074/jbc.M806881200.
[89] T. Kamiya, T. Fujiwara, Arabidopsis NIP1;1 transports antimonite and determines antimonite sensitivity, Plant Cell Physiol 50 (2009) 1977–1981. https://doi.org/10.1093/pcp/pcp130.
[90] S. Vats, S. Sudhakaran, A. Bhardwaj, R. Mandlik, Y. Sharma, S. Kumar, D.K. Tripathi, H. Sonah, T.R. Sharma, R. Deshmukh, Targeting aquaporins to alleviate hazardous metal(loid)s imposed stress in plants, J. Hazard. Mater. 408 (2021) 16. https://doi.org/10.1016/j.jhazmat.2020.124910.
[91] M.A. Macho-Rivero, M.B. Herrera-Rodríguez, R. Brejcha, A.R. Schäffner, N. Tanaka, T. Fujiwara, A. González-Fontes, J.J. Camacho-Cristóbal, Boron Toxicity Reduces Water Transport from Root to Shoot in Arabidopsis Plants. Evidence for a Reduced Transpiration Rate and Expression of Major PIP Aquaporin Genes, Plant Cell Physiol 59 (2018) 836–844. https://doi.org/10.1093/pcp/pcy026.
[92] H.K. Lee, S.K. Cho, O. Son, Z. Xu, I. Hwang, W.T. Kim, Drought Stress-Induced Rma1H1, a RING Membrane-Anchor E3 Ubiquitin Ligase Homolog, Regulates Aquaporin Levels via Ubiquitination in Transgenic Arabidopsis Plants, The Plant Cell 21 (2009) 622–641. https://doi.org/10.1105/tpc.108.061994.
[93] Q. Chen, R. Liu, Y. Wu, S. Wei, Q. Wang, Y. Zheng, R. Xia, X. Shang, F. Yu, X. Yang, L. Liu, X. Huang, Y. Wang, Q. Xie, ERAD-related E2 and E3 enzymes modulate the drought response by regulating the stability of PIP2 aquaporins, Plant Cell 33 (2021) 2883–2898. https://doi.org/10.1093/plcell/koab141.
[94] N. Berger, V. Demolombe, S. Hem, V. Rofidal, L. Steinmann, G. Krouk, A. Crabos, P. Nacry, L. Verdoucq, V. Santoni, Root Membrane Ubiquitinome under Short-Term Osmotic Stress, Int J Mol Sci 23 (2022) 1956. https://doi.org/10.3390/ijms23041956.
[95] V.G. Doblas, E. Smakowska-Luzan, S. Fujita, J. Alassimone, M. Barberon, M. Madalinski, Y. Belkhadir, N. Geldner, Root diffusion barrier control by a vasculature-derived peptide binding to the SGN3 receptor, Science 355 (2017) 280–284. https://doi.org/10.1126/science.aaj1562.
[96] T. Nakayama, H. Shinohara, M. Tanaka, K. Baba, M. Ogawa-Ohnishi, Y. Matsubayashi, A peptide hormone required for Casparian strip diffusion barrier formation in Arabidopsis roots, Science 355 (2017) 284–286. https://doi.org/10.1126/science.aai9057.
[97] P. Wang, M. Calvo-Polanco, G. Reyt, M. Barberon, C. Champeyroux, V. Santoni, C. Maurel, R.B. Franke, K. Ljung, O. Novak, N. Geldner, Y. Boursiac, D.E. Salt, Surveillance of cell wall diffusion barrier integrity modulates water and solute transport in plants, Sci Rep 9 (2019) 4227. https://doi.org/10.1038/s41598-019-40588-5.
[98] M. Calvo-Polanco, Z. Ribeyre, M. Dauzat, G. Reyt, C. Hidalgo-Shrestha, P. Diehl, M. Frenger, T. Simonneau, B. Muller, D.E. Salt, R.B. Franke, C. Maurel, Y. Boursiac, Physiological roles of Casparian strips and suberin in the transport of water and solutes, New Phytologist 232 (2021) 2295–2307. https://doi.org/10.1111/nph.17765.

Figure legends

Figure 1. Quantification of U in soluble and membrane fractions from Arabidopsis roots.
(**A**) Immunodetection of the tonoplast intrinsic protein (TIP1;1, TIP1;2) and plastid fructose-bisphosphate aldolases (FBAs) in soluble (S) and SDS-solubilized (membrane, M) fractions extracted from Arabidopsis roots. One replicate of the experiment is show (untreated plants, samples R-0-2s and R-0-2m). SDS-PAGE and immunoblot analysis of all replicates are shown in Figures S2 and S3. (**B**) Uranium concentration in the soluble and membrane fractions. Proteins fractions were mineralized with nitric acid and U was quantified by ICP-MS. Bar plots represent mean ± SD with n=6 biological replicates. (**C**) Uranium distribution between the soluble and membrane fractions. Values calculated from the data in (B) and the distribution of proteins in the soluble fractions (13 ± 2%) and SDS-solubilized fractions (87 ± 2%). Data are mean ± SD of n=6 biological replicates. The non-parametric Tukey test showed a significant difference in U content between soluble and membrane fractions at both U5 and U50, with p <0.01.

Figure 2. Clustering of proteins according to their accumulation patterns in response to U stress.
Clustering was calculated by the SOTA method using Z-score transformed values to identify homogeneous patterns of protein abundance changes. Eight clusters (CL1 to CL8) have been defined to illustrate the main protein accumulation patterns in response to U stress. Individual profiles are depicted by gray lines (Z-score), the average profile is marked in red. The number of proteins in each cluster is indicated.

Figure 3. GO enrichment analysis of cellular components regulated by U stress.
GO enrichment analysis of cellular components was performed with the 458 DAPs using the (**A**) BiNGO and (**B**) Metascape tools. Bubble plots show GO terms ordered by enrichment factors (threshold >2.3 for BiNGO, >3 for Metascape). BiNGO settings to assess overrepresented GO cellular components were as follows: statistical hypergeometric test, Bonferroni Family-Wise Error rate multiple testing correction, and significant *p*-value <0.05. Genes were annotated with plant GO slim terms. The Metascape enrichment analysis has been done with the GO cellular components ontology source. Terms with a *p*-value <0.01, a minimum count of 3, and an enrichment factor >1.5 have been grouped into clusters based on their membership similarities.

Figure 4. Protein classes and metal cofactors associated with differentially accumulated proteins under U stress.
Circular diagrams representing (**A**) the proportion of the different protein classes and (**B**) the nature of cofactors associated with the identified proteins. Fe: iron, Ca: calcium, Zn: zinc, Mg: magnesium, Cu:

copper, Mn: manganese, Co: cobalt, Ni: nickel, ?: unknown metal.

Figure 5. GO enrichment analysis of biological processes regulated by U stress.

GO enrichment analysis of biological processes was performed with the 458 DAPs using the (**A**) BiNGO and (**B**) Metascape tools. Bubble plots show GO terms grouped by major functions (threshold >1.8 for BiNGO, >2.2 for Metascape). BiNGO settings to assess overrepresented biological processes were statistical hypergeometric test, Bonferroni Family-Wise Error rate multiple testing correction, and significant *p*-value <0.05. The Metascape enrichment analysis has been done with the GO biological processes ontology source. Terms with a *p*-value <0.01, a minimum count of 3, and an enrichment factor >1.5 have been grouped into clusters based on their membership similarities.

Figure 6. Heatmaps representing sets of proteins regulated by U stress.

Proteins whose abundance is significantly (*p*-value <0.05) increased or decreased in response to U stress are shown in red and green, respectively. Protein changes not supported by *p*-value <0.05 are in white. Expression levels values are in log2 scale. (**A**) stress, (**B**) cell wall organization, (**C**) vesicular transport, (**D**) solute transport.

Figure 7. Accumulation profiles of the U-binding proteins PCaP1 and GRP7 in response to U stress.

(**A**) Immunodetection of PCap1 and GRP7. Proteins were resolved by SDS-PAGE, transferred to PVDF membranes and immunodetected using antibodies to PCaP1 and GRP7 from Arabidopsis. Protein loading onto the gel was assessed by Coomassie Brilliant Blue staining. (**B**) Abundance of PCaP1 and GRP7 according to proteomic data. Boxplots show the Log(abundance) of the proteins from 6 biological replicates. Letters indicate statistical differences according to a Tukey test (*p*-value <0.05).

Figure 8: Root hydraulic conductivity and leaf transpiration rate measurements in Arabidopsis under U stress

(**A**) Effect of U on root hydraulic conductivity. $L p_r$ was measured in pressure chambers using excised roots from Arabidopsis plants in control condition (U0) or challenged with 50 µM uranyl nitrate (U50) for 24 h. Sodium azide was used to discriminated the aquaporin-dependent (NaN_3 sensitive) and –independent components of $L p_r$. Data represent one experiment from two independent replicates. Bar plots represent mean ± SD with n=7-12. Letters indicate statistical differences according to a non-parametric Mann-Whitney test. Capital letters are for aquaporin-related $L p_r$ (*p*-value <0.0001), lowercase for residual $L p_r$ (*p*-value >0.05). (**B**) Effect of U on leaf transpiration rate. Plants cultivated in control condition (U0) or with 50 µM uranyl nitrate (U50) were weighted every 3.5 h during the light phase over a 2-day period and leaf transpiration rates per hour were normalized to rosette leaf area.

Data represent one experiment from two independent replicates. Each data point is presented as the mean ± SD with n=4.

Supplementary material

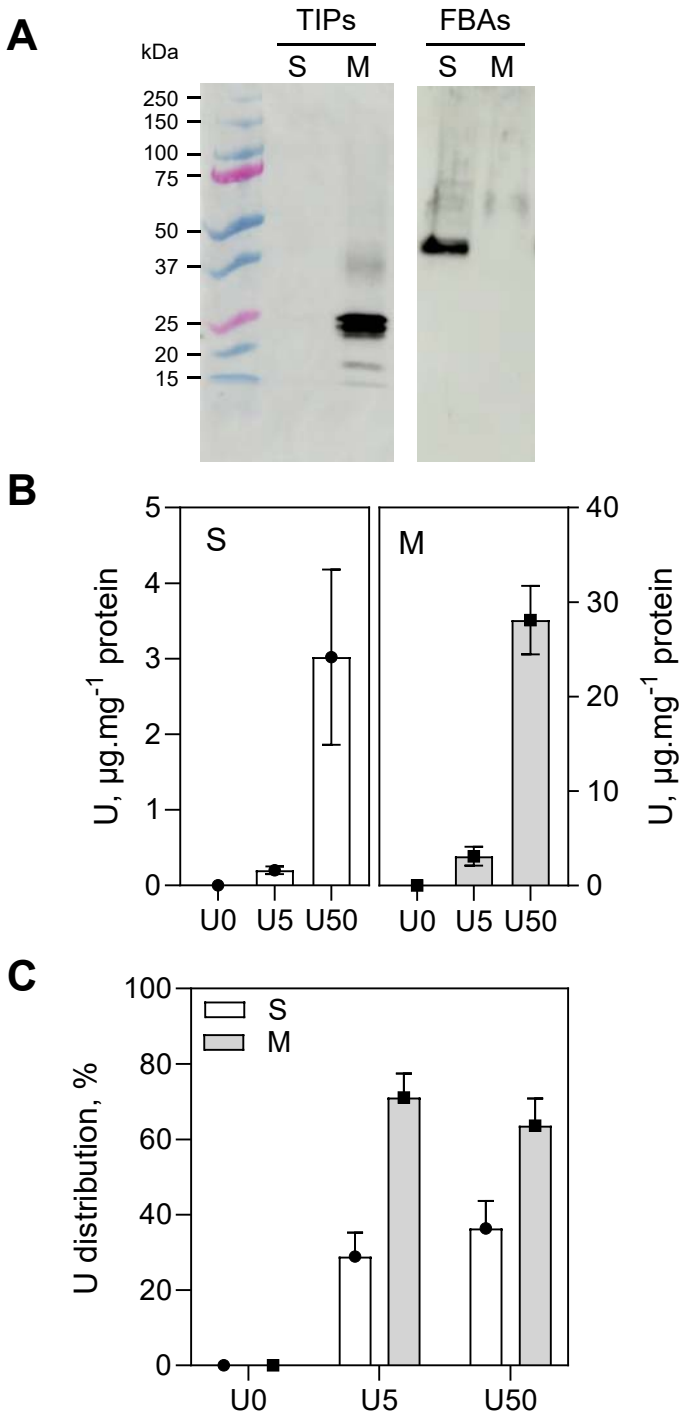

Figure 1. Quantification of U in soluble and membrane fractions from Arabidopsis roots.

(**A**) Immunodetection of the tonoplast intrinsic protein (TIP1;1, TIP1;2) and plastid fructose-bisphosphate aldolases (FBAs) in soluble (S) and SDS-solubilized (membrane, M) fractions extracted from Arabidopsis roots. One replicate of the experiment is show (untreated plants, samples R-0-2s and R-0-2m). SDS-PAGE and immunoblot analysis of all replicates are shown in Figures S2 and S3. (**B**) Uranium concentration in the soluble and membrane fractions. Proteins fractions were mineralized with nitric acid and U was quantified by ICP-MS. Bar plots represent mean ± SD with n=6 biological replicates. (**C**) Uranium distribution between the soluble and membrane fractions. Values calculated from the data in (B) and the distribution of proteins in the soluble fractions (13 ± 2%) and SDS-solubilized fractions (87 ± 2%). Data are mean ± SD of n=6 biological replicates.

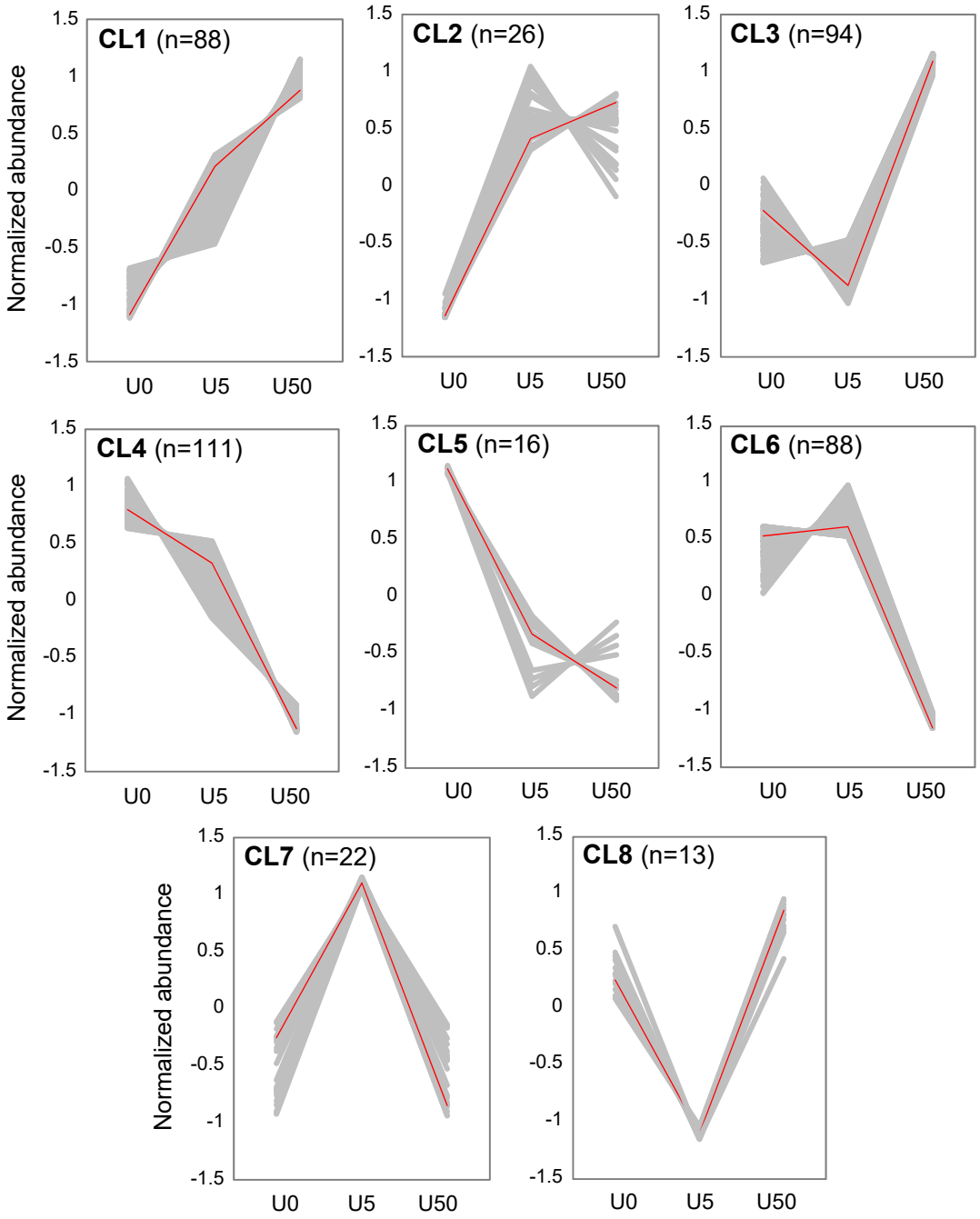

Figure 2. Clustering of proteins according to their accumulation patterns in response to U stress.

Clustering was calculated by the SOTA method using Z-score transformed values to identify homogeneous patterns of protein abundance changes. Eight clusters (CL1 to CL8) have been defined to illustrate the main protein accumulation patterns in response to U stress. Individual profiles are depicted by gray lines (Z-score), the average profile is marked in red. The number of proteins in each cluster is indicated.

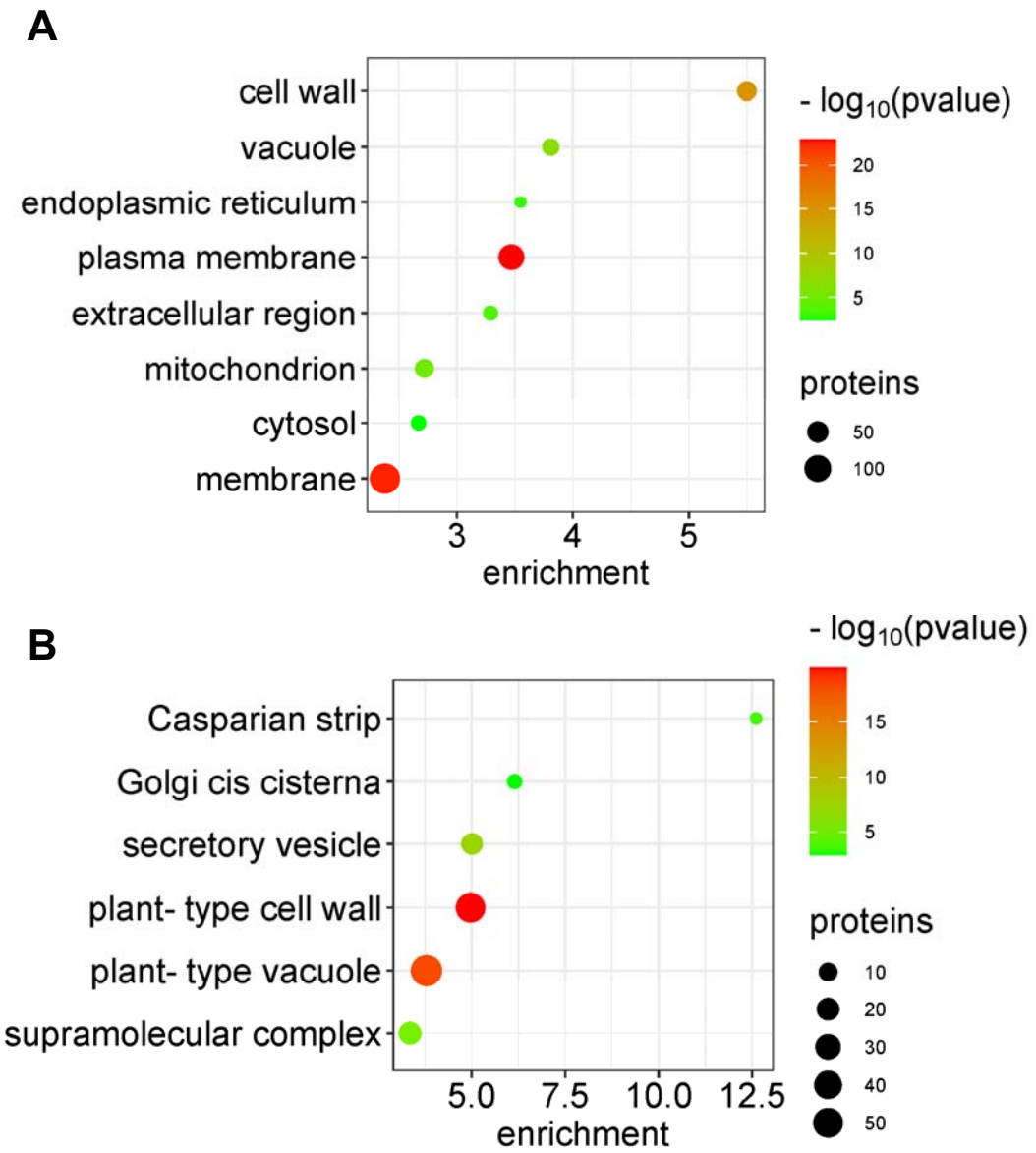

Figure 3. GO enrichment analysis of cellular components regulated by U stress.
GO enrichment analysis of cellular components was performed with the 458 DAPs using the (**A**) BiNGO and (**B**) Metascape tools. Bubble plots show GO terms ordered by enrichment factors (threshold >2.3 for BiNGO, >3 for Metascape). BiNGO settings to assess overrepresented GO cellular components were as follows: statistical hypergeometric test, Bonferroni Family-Wise Error rate multiple testing correction, and significant p-value <0.05. Genes were annotated with plant GO slim terms. The Metascape enrichment analysis has been done with the GO cellular components ontology source. Terms with a p-value <0.01, a minimum count of 3, and an enrichment factor >1.5 have been grouped into clusters based on their membership similarities.

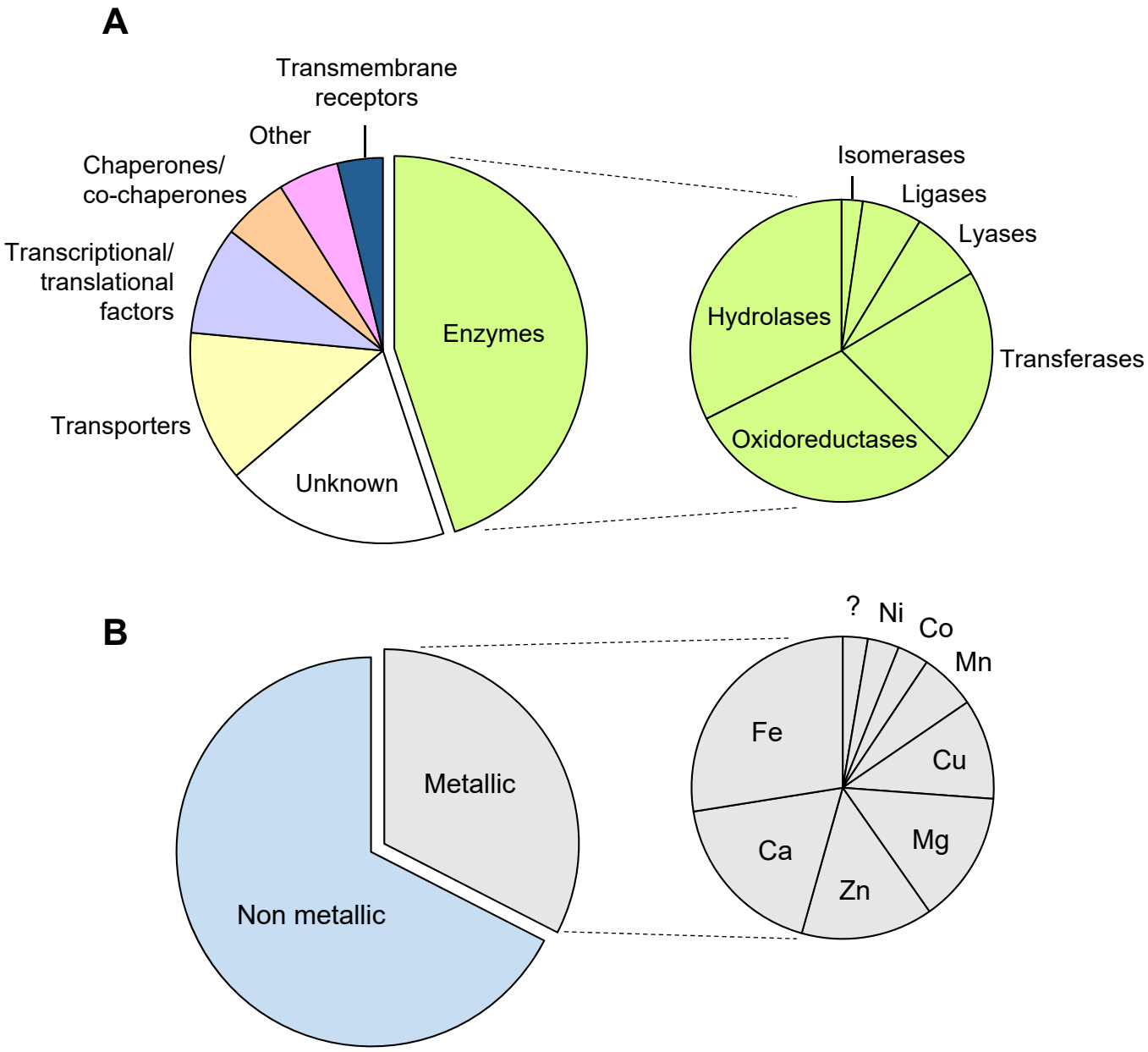

Figure 4. Protein classes and metal cofactors associated with differentially accumulated proteins under U stress.
Circular diagrams representing (**A**) the proportion of the different protein classes and (**B**) the nature of cofactors associated with the identified proteins. Fe: iron, Ca: calcium, Zn: zinc, Mg: magnesium, Cu: copper, Mn: manganese, Co: cobalt, Ni: nickel, ?: unknown metal.

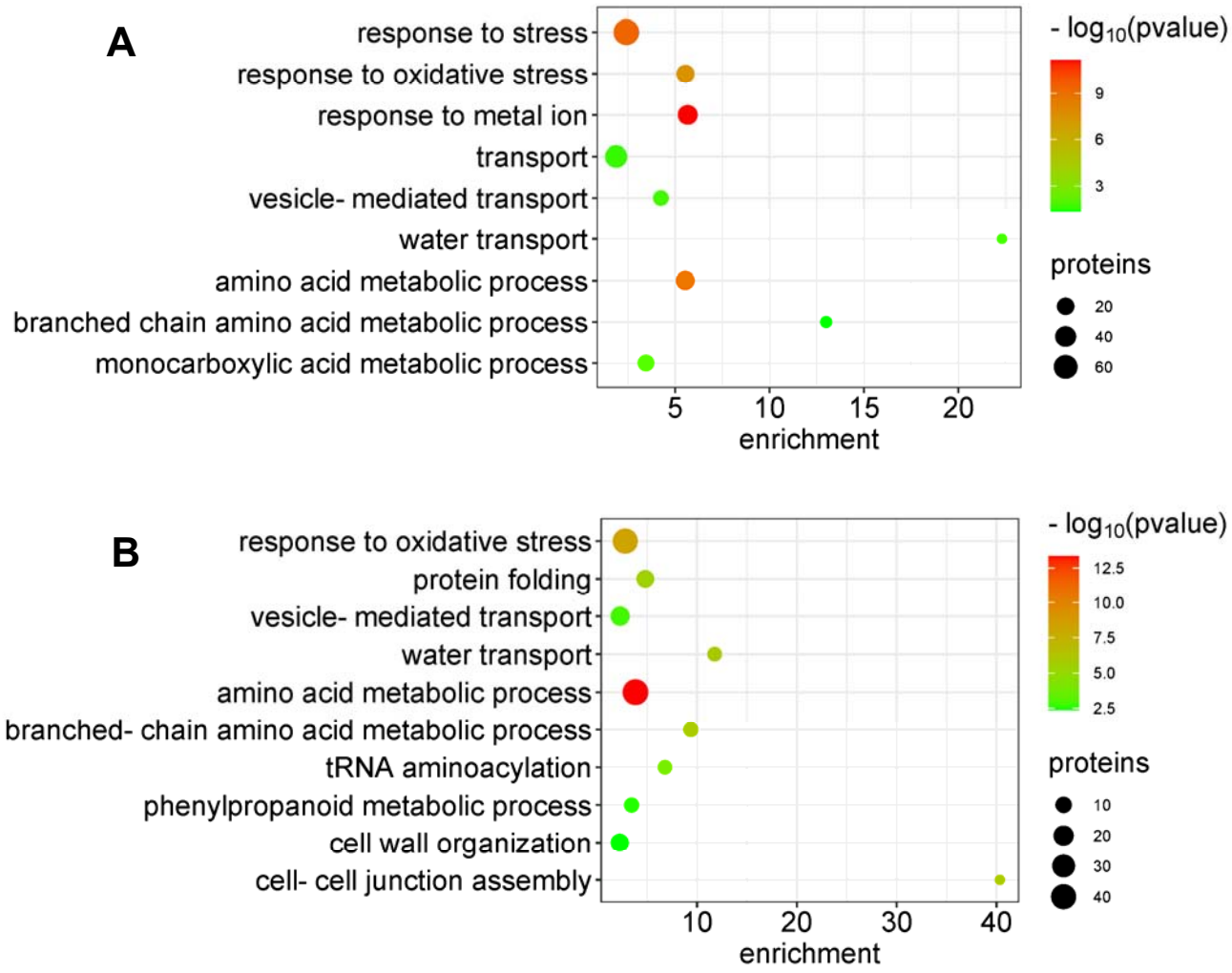

Figure 5. GO enrichment analysis of biological processes regulated by U stress.
GO enrichment analysis of biological processes was performed with the 458 DAPs using the (**A**) BiNGO and (**B**) Metascape tools. Bubble plots show GO terms grouped by major functions (threshold >1.8 for BiNGO, >2.2 for Metascape). BiNGO settings to assess overrepresented biological processes were statistical hypergeometric test, Bonferroni Family-Wise Error rate multiple testing correction, and significant p-value <0.05. The Metascape enrichment analysis has been done with the GO biological processes ontology source. Terms with a p-value <0.01, a minimum count of 3, and an enrichment factor >1.5 have been grouped into clusters based on their membership similarities.

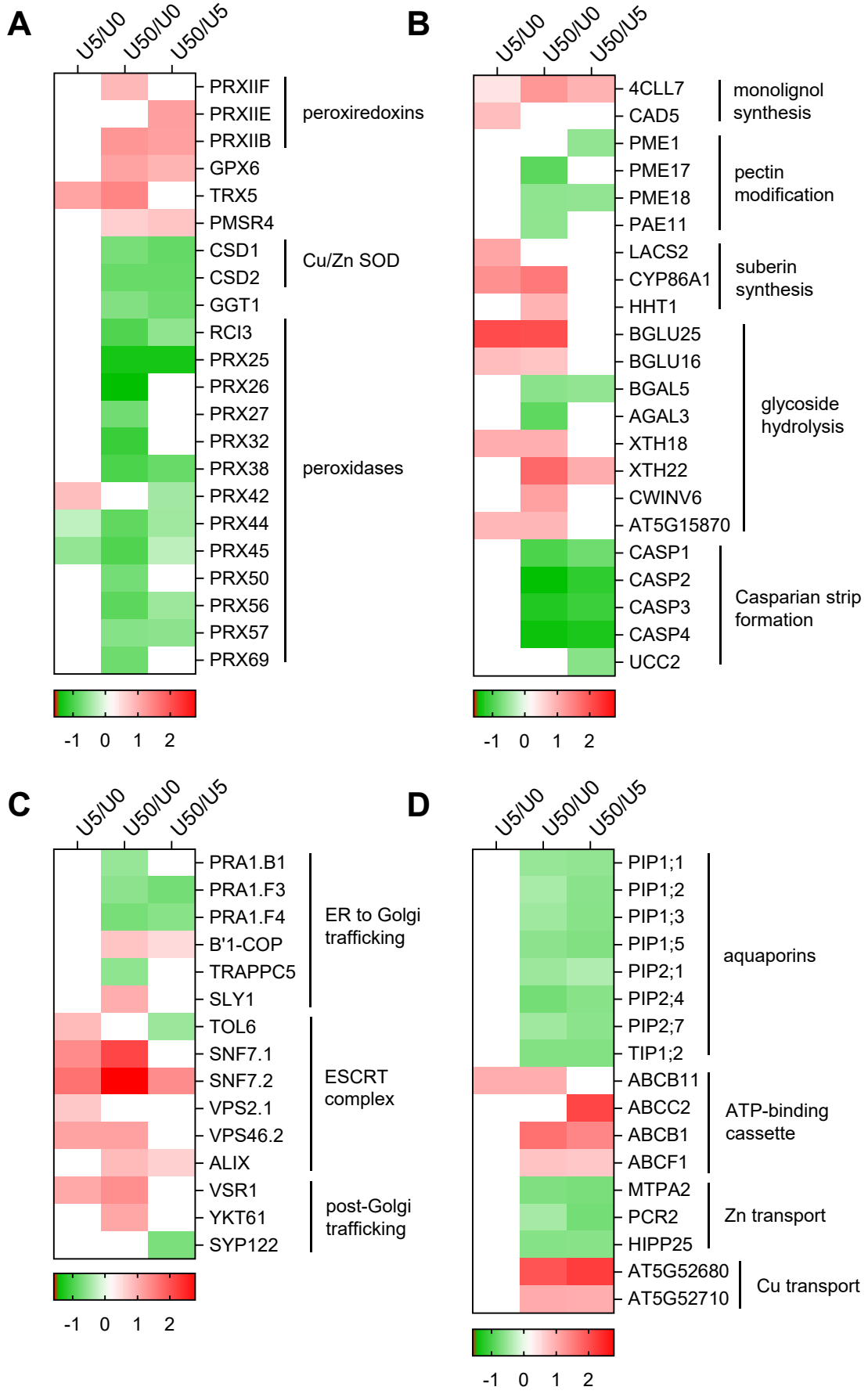

Figure 6. Heatmaps representing sets of proteins regulated by U stress.
Proteins whose abundance is significantly ($p<0.05$) increased or decreased in response to U stress are shown in red and green, respectively. Protein changes not supported by $p<0.05$ are in white. Expression levels values are in log2 scale. (**A**) stress, (**B**) cell wall organization, (**C**) vesicular transport, (**D**) solute transport.

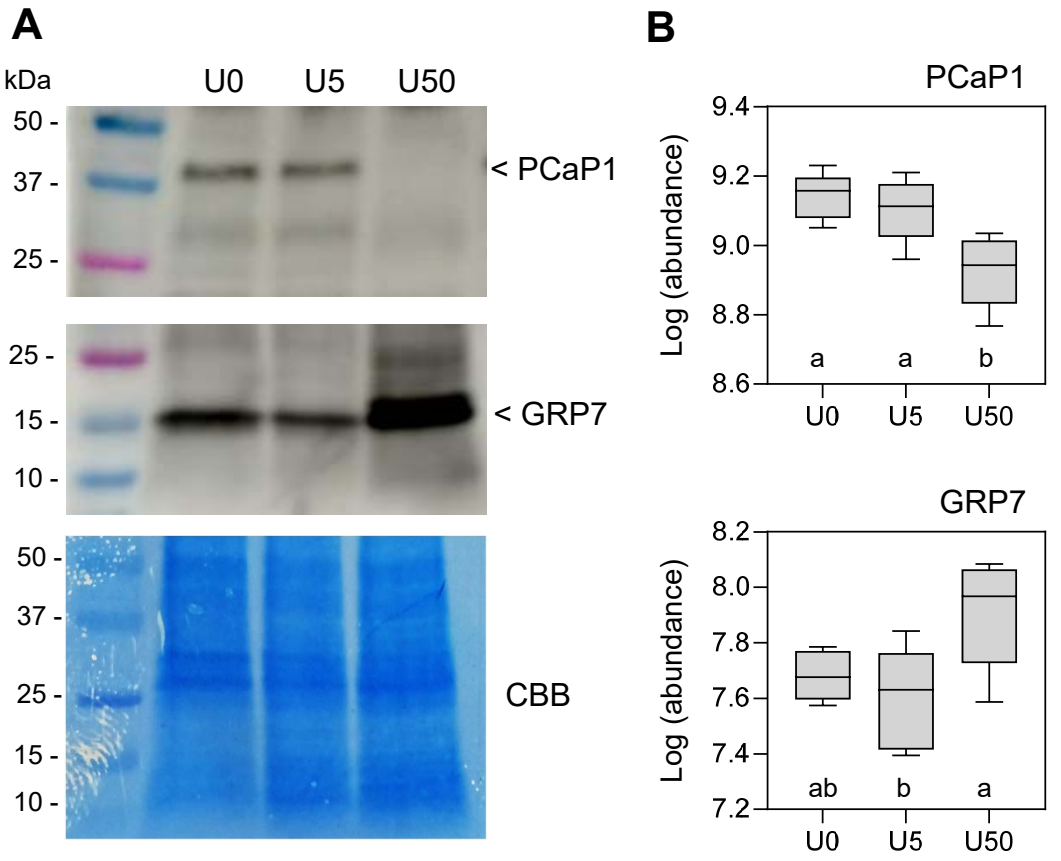

Figure 7. Accumulation profiles of the U-binding proteins PCaP1 and GRP7 in response to U stress.

(**A**) Immunodetection of PCap1 and GRP7. Proteins were resolved by SDS-PAGE, transferred to PVDF membranes and immunodetected using antibodies to PCaP1 and GRP7 from Arabidopsis. Protein loading on the gel was assessed by Coomassie Brilliant Blue staining. (**B**) Abundance of PCaP1 and GRP7 according to proteomic data. Boxplots show the Log(abundance) of the proteins from 6 biological replicates. Letters indicate statistical differences according to a Tukey test ($p<0.05$).

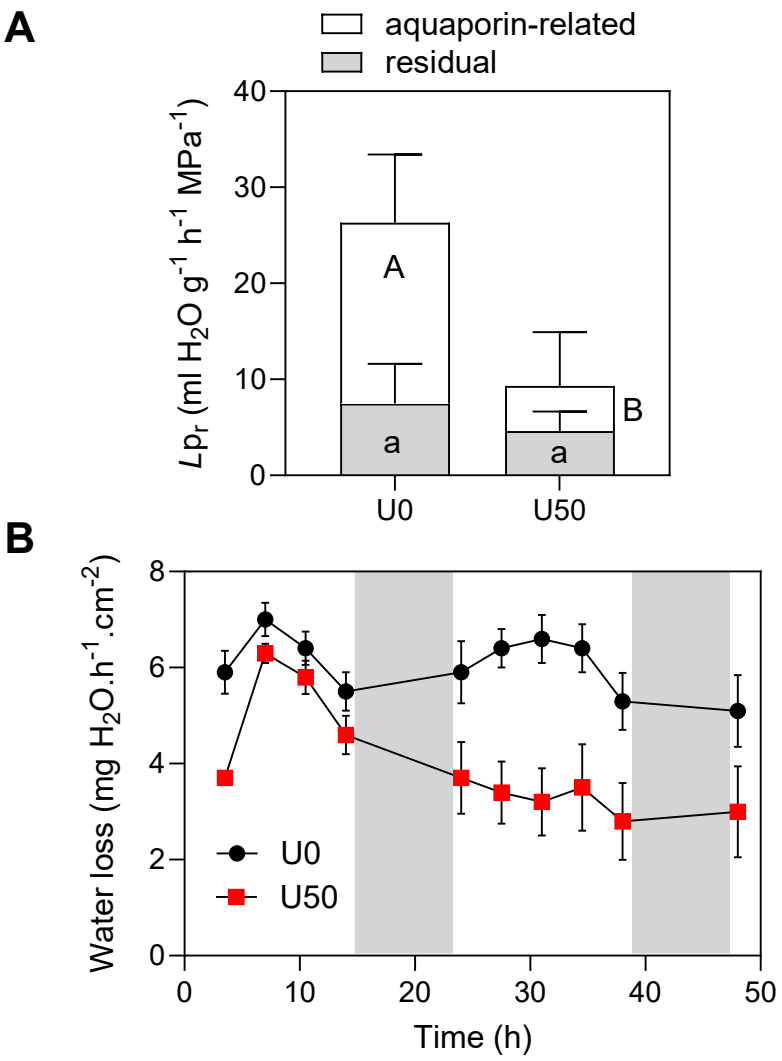

Figure 8. Root hydraulic conductivity and leaf transpiration rate measurements in Arabidopsis under U stress

(**A**) Effect of U on root hydraulic conductivity. Lp_r was measured in pressure chambers using excised roots from Arabidopsis plants in control condition (U0) or challenged with 50 µM uranyl nitrate (U50) for 24h. Sodium azide was used to discriminated the aquaporin-dependent (NaN_3 sensitive) and –independent components of Lp_r. Data represent one experiment from two independent replicates. Bar plots represent mean ± SD with n=7-12. Letters indicate statistical differences according to a non-parametric Mann-Whitney test. Capital letters are for aquaporin-related Lp_r ($p<0.0001$), lowercase for residual Lp_r ($p>0.05$). (**B**) Effect of U on leaf transpiration rate. Plants cultivated in control condition (U0) or with 50 µM uranyl nitrate (U50) were weighted every 3.5 h during the light phase over a 2-day period and leaf transpiration rates per hour were normalized to rosette leaf area. Data represent one experiment from two independent replicates. Each data point is presented as the mean ± SD with n=4.

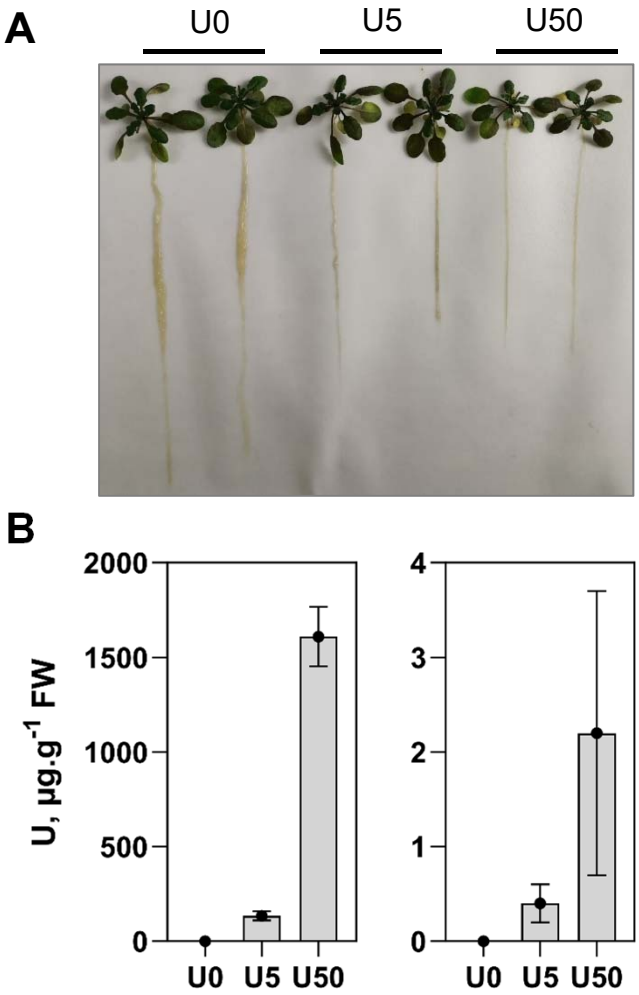

Figure S1. Uranium concentration in roots and shoots of Arabidopsis plants.
(**A**) Morphological characteristics of 30-day-old Arabidopsis plants exposed to uranyl nitrate for 48 h. Two representative control (U0) and U-treated plants (U5 and U50 for 5 and 50 µM uranyl nitrate, respectively) are shown. (**B**) Uranium concentration in roots (left panel) and shoots (right panel). Uranium was measured by ICP-MS in mineralized samples. Data are mean ± SD of n=6 biological replicates. The non-parametric Tukey test showed a significant difference in U content between roots and shoots at both U5 and U50 treatments, with $p<0.01$.

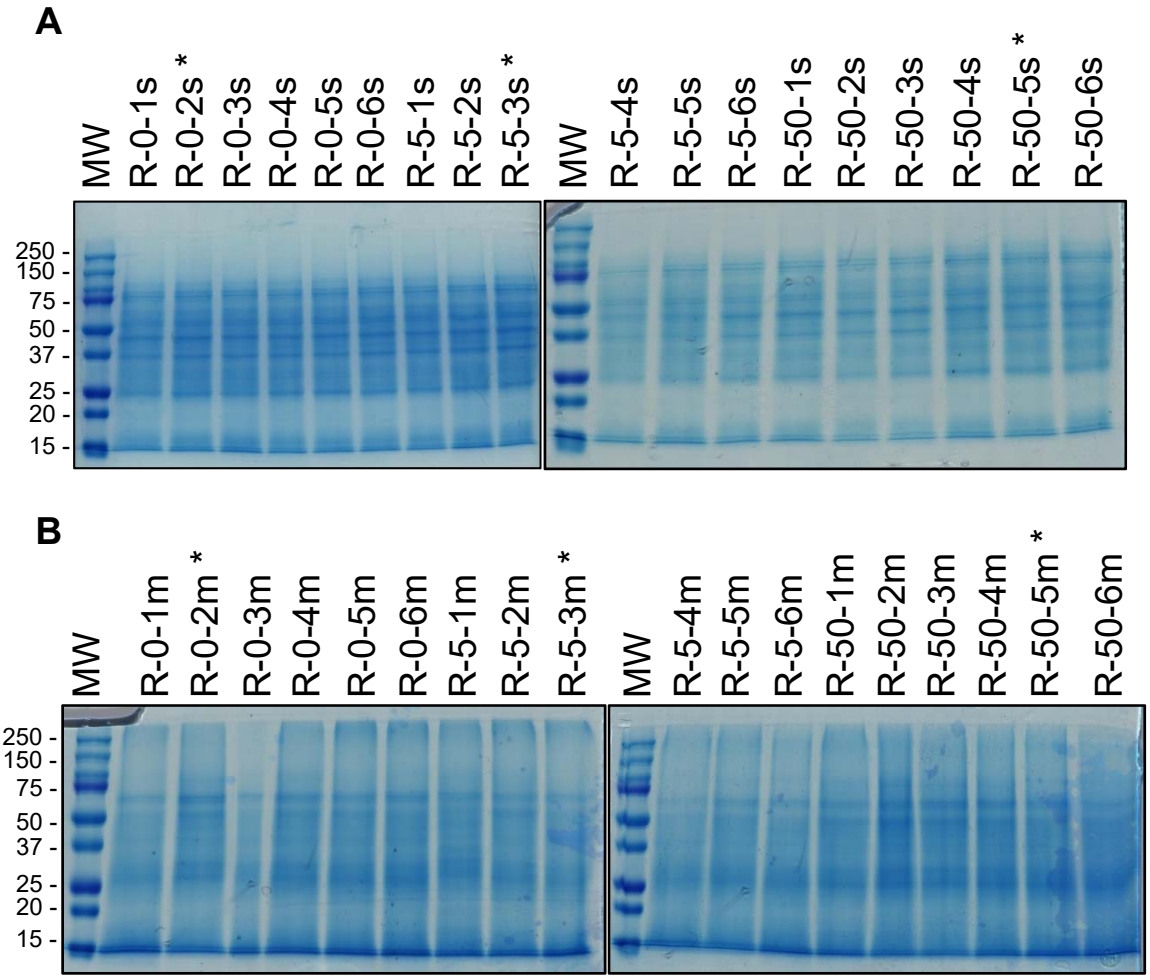

Figure S2. SDS-PAGE analysis of soluble and membrane proteins from Arabidopsis roots.

SDS-PAGE analysis of (**A**) soluble and (**B**) membrane proteins from control and U-treated *A. thaliana* roots. Proteins were stained with Coomassie Blue. Sample nomenclature: R, root; U concentration (0, 5 ,50 µM uranyle nitrate): 1s to 6s, biological replicates of soluble protein extracts; m1 to m6, biological replicates of membrane protein extracts; *, samples analyzed by immunoblot (Figure S3).

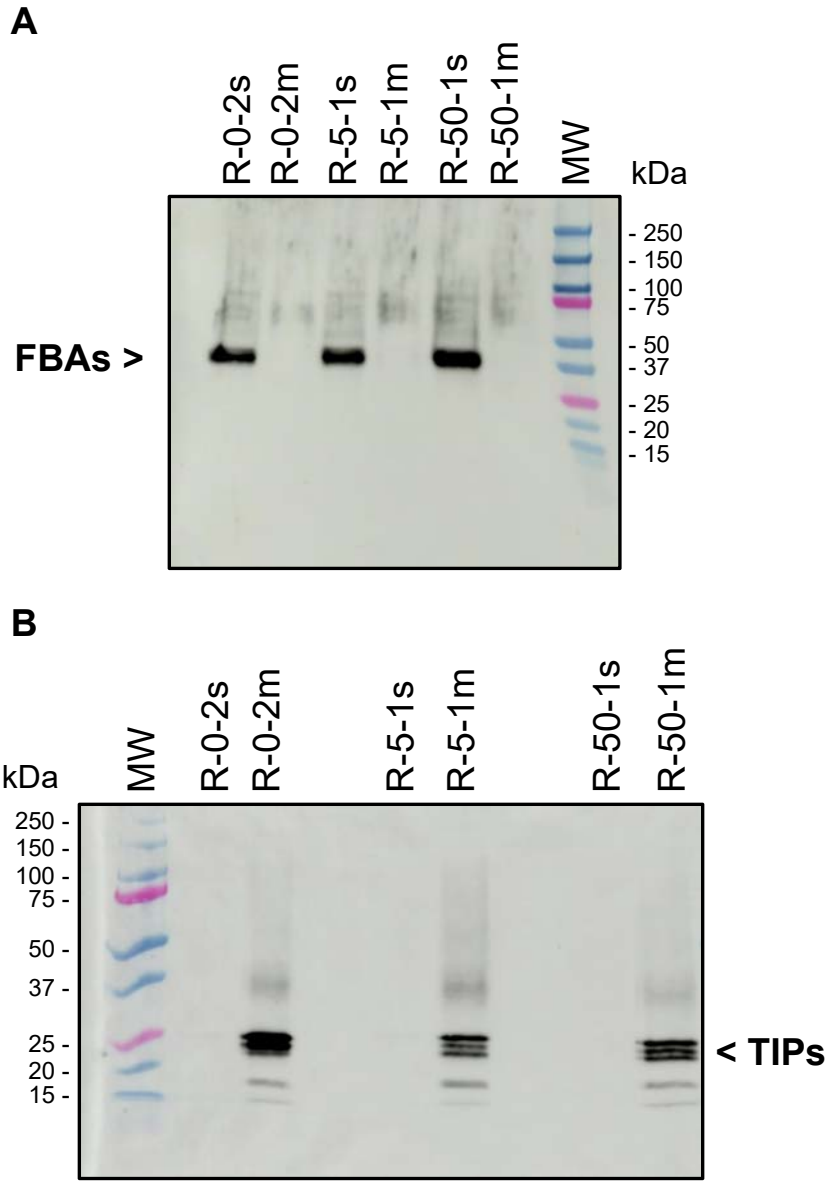

Figure S3. Quality assessment of membrane proteins from Arabidopsis roots by Western blot analysis.
Immunodetection of (**A**) the fructose-bisphosphate aldolases (FBAs) and (**B**) the tonoplastic intrinsic protein (TIP1;1, TIP1;2) in soluble (s) and membrane (m) protein extracts isolated from roots of Arabidopsis plants treated with 0, 5 and 50 µM uranyl nitrate. SDS-PAGE analysis of protein extracts (including sample nomenclature) is shown in Figure S2.

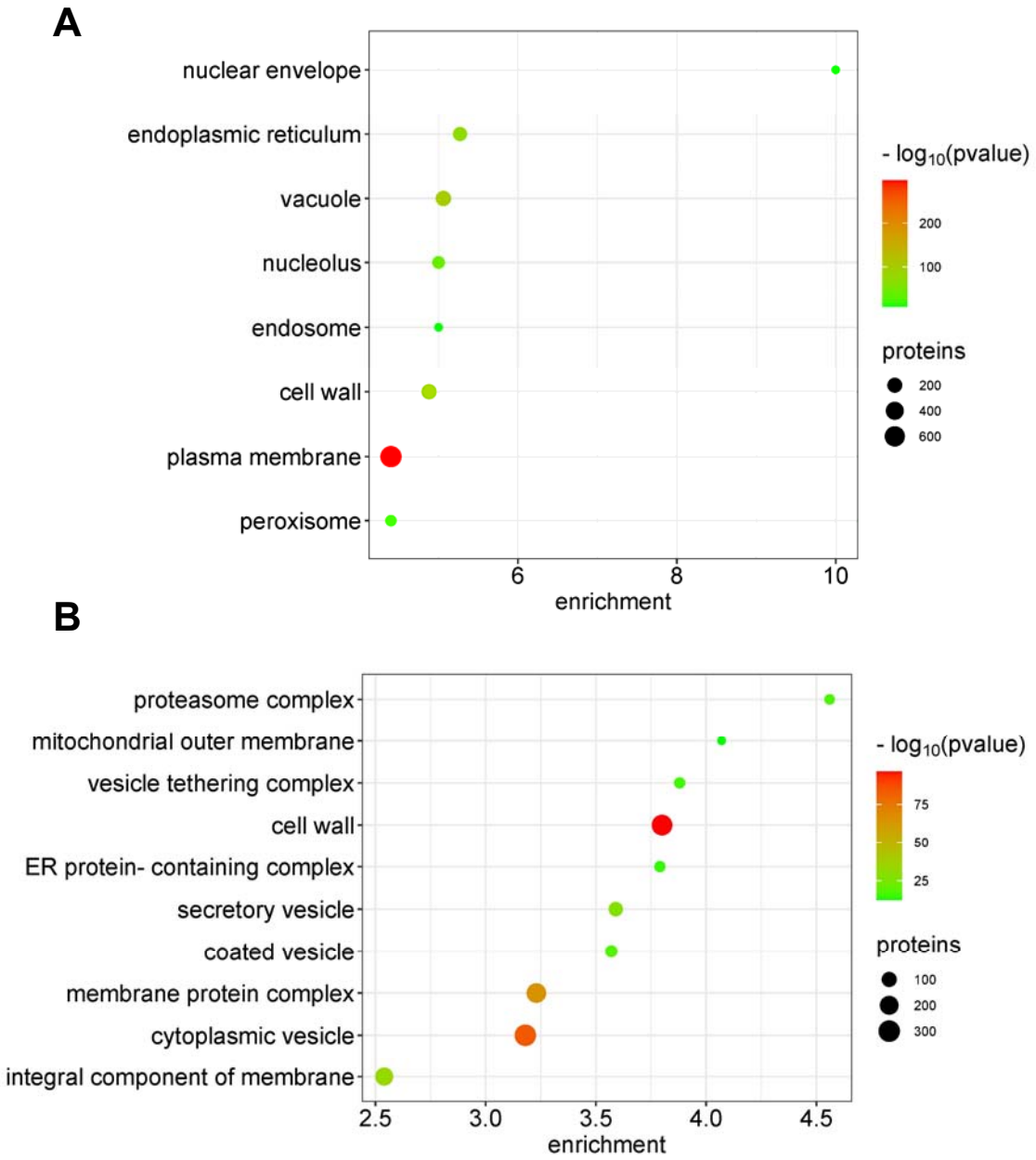

Figure S4. GO enrichment analysis of cellular components in the membrane and cell wall proteome of Arabidopsis roots.
GO enrichment analysis of cellular components was performed using the 2,802 proteins identified by mass spectrometry using the BiNGO (**A**) and Metascape (**B**) tools. Bubble plots show GO terms ordered by enrichment values (threshold >4 for BiNGO, >2.5 for Metascape). BiNGO settings to assess overrepresented GO cellular components were as follows: statistical hypergeometric test, Bonferroni Family-Wise Error rate multiple testing correction, and significant p-value <0.05. The Metascape enrichment analysis has been done with the GO cellular components ontology source. Terms with a p-value <0.01, a minimum count of 3, and an enrichment factor >2.0 have been grouped into clusters based on their membership similarities.

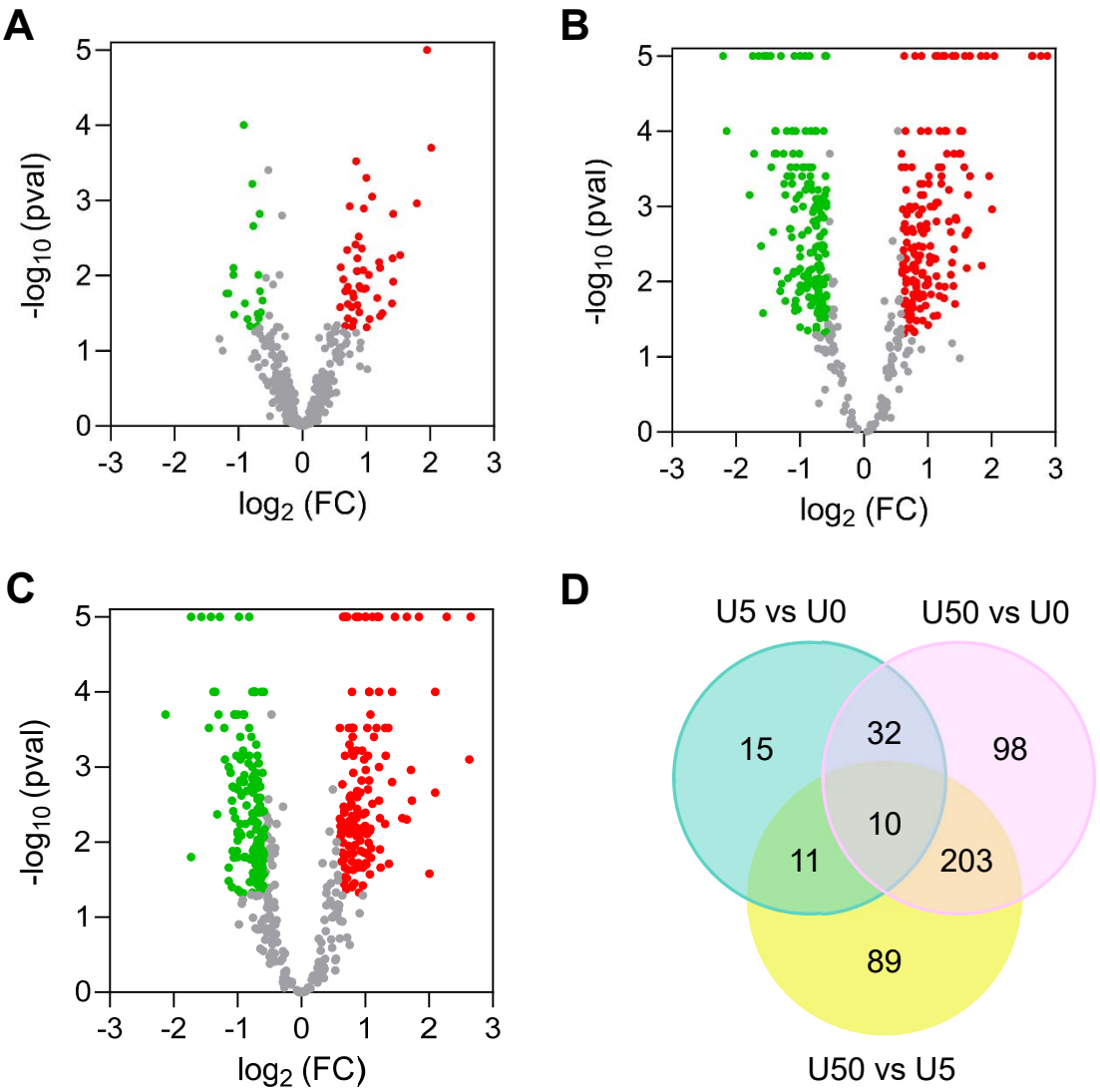

Figure S5. Differential accumulation of root membrane proteins in response to U stress. The relative abundance of root membrane proteins was compared in conditions U5 vs U0 (**A**), U50 vs U0 (**B**), and U50 vs U5 (**C**). Differentially accumulated proteins were defined using a fold change threshold >1.5 and a p-value <0.05 (Tukey test). In volcano plots, down-regulated and up-regulated proteins are shown in green and red, respectively. Proteins considered not regulated by U (fold change ≤1.5 and/or pvalue ≥0.05) are in grey. Proteins with p-value = 0 (Tukey test) were plotted with a –log10 (pval) of 5 for convenient graphical display. The Venn diagram (**D**) summarizes the number of DAPs in the three comparisons. Data are representative of six independent experiments.

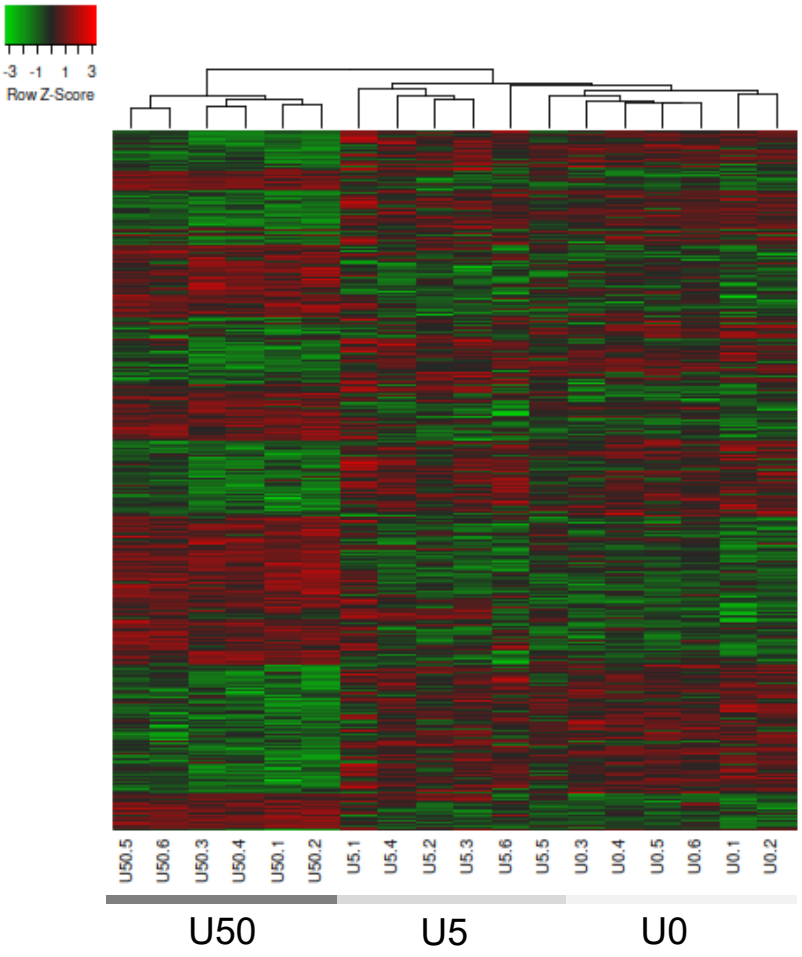

Figure S6. Global accumulation profiles of *A. thaliana* root membrane proteins in response to U stress.

The heatmap represents the 458 proteins showing a significant change in abundance when exposed to 5 or 50 µM uranyl nitrate. Clustering was performed using the Heatmapper expression server with the average linkage clustering method and the Euclidean distance measurement method. Z-score normalization of protein expression values was done prior to clustering.

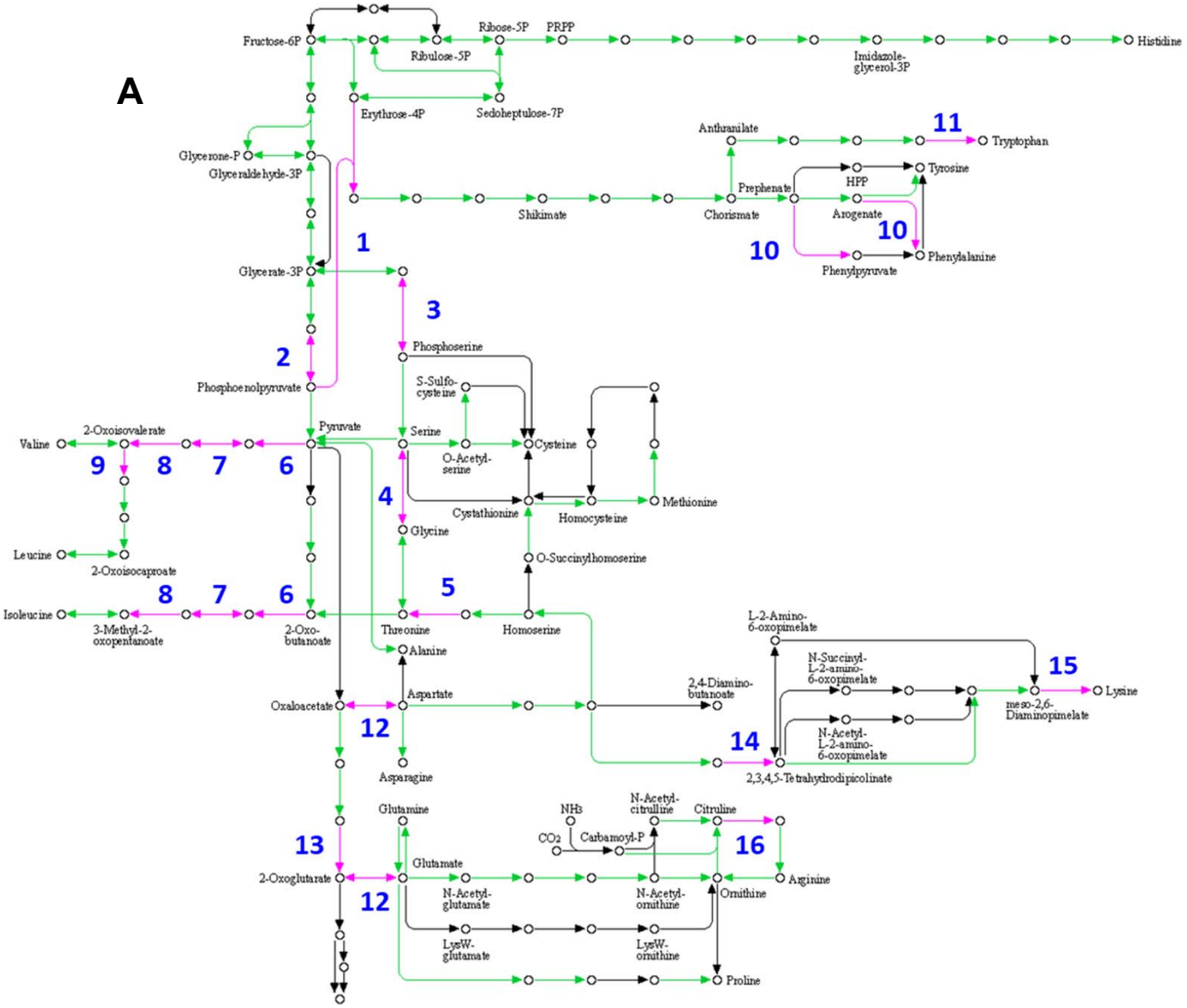

Figure S7. Effect of U on amino acid metabolism.
(**A**) Proteins regulated by U are mapped to the KEGG pathway 'biosynthesis of amino acids' (ath01230). (**B**) Protein expression profiles are shown on a heatmap. The numbers in brackets refer to the enzyme positions in the pathway. (**C**) Heatmap of tRNA ligases regulated during U stress (not indicated on the pathway). Proteins whose abundance is significantly ($p<0.05$) increased or decreased in response to U stress are shown in red and green, respectively (log2 scale).

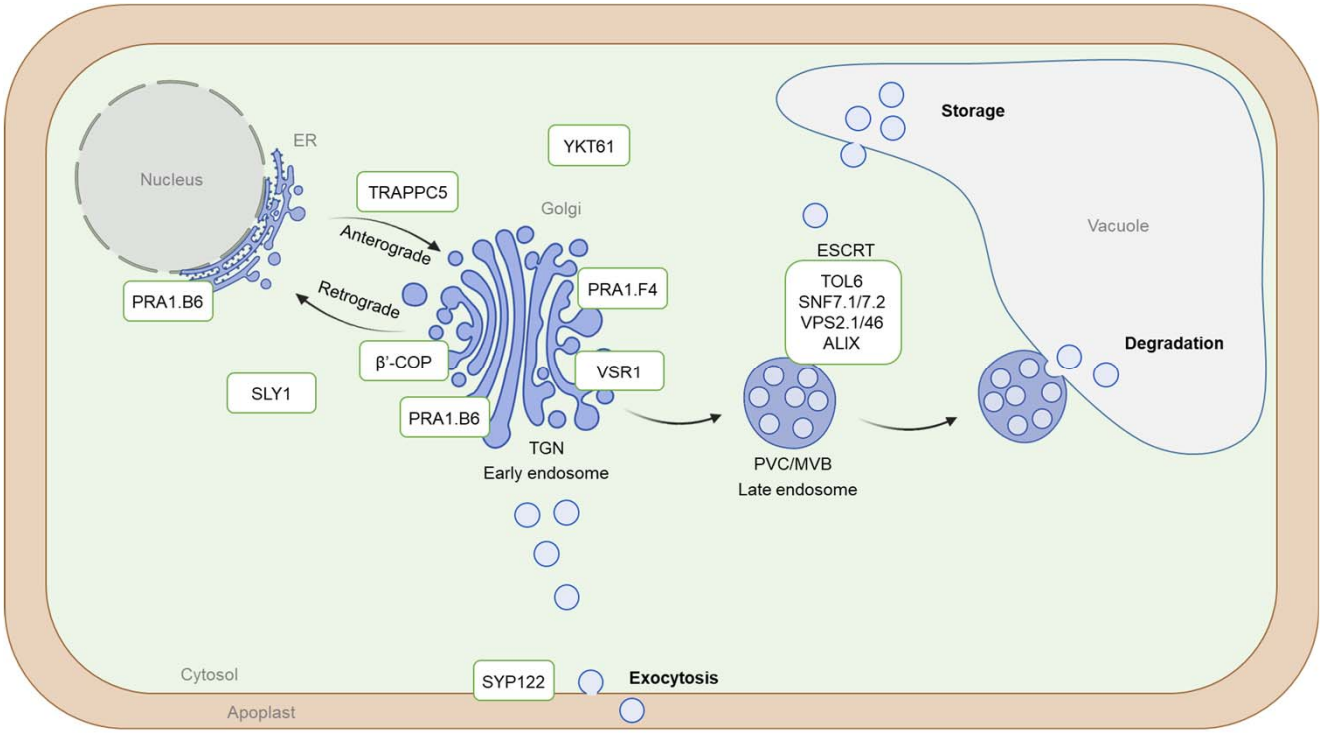

Figure S8. Endomembrane trafficking proteins differentially regulated by U.
PRA1s play a role in the trafficking of cargo proteins destined to various endomembrane compartments [97,98]. AtPRA1.B6 is localized to the ER and the Golgi [97], PRA1.F4 is found in the Golgi [99] whereas the subcellular localization of AtPRA1.B1 has not been demonstrated. SLY1, by acting in the ER and Golgi, could contribute to membrane fusion by interacting with Qa-SNAREs or nascent trans-SNARE complexes [100]. The COPI coat composed of seven subunits (α/β/β'/γ/δ/ε/ζ) interacts with Golgi membranes [101]. The coatomer complex is not only involved in the biogenesis of COPI vesicles but it is also required to select the cargo to be included in the vesicles. Coat protein I (COPI) is necessary for intra-Golgi transport and retrograde transport from the Golgi back to the ER [102]. TRAPPC5 belongs to TRAPPI which functions in ER to Golgi transport [104]. YKT61 is a unique R-SNARE lacking transmembrane domains[100]. Thus, it is present mainly in the cytoplasm and is critical for the dynamic biogenesis of vacuoles, for the maintenance of Golgi morphology, and for endocytosis, suggesting a broad role of YKT61-mediated vesicular trafficking in plant development [105]. VSR1 is responsible for the sorting of proteins from the trans-Golgi network (TGN) to prevacuolar compartments (PVCs) and finally to their respective vacuoles [106]. The ESCRT machinery is responsible for the recruitment of the ubiquitinated cargo and membrane budding for ILV formation. Ubiquitinated cargoes are captured by ESCRT-0-like proteins, TOLs. The cargoes are subsequently translocated to the ESCRT-I, ESCRT-II and ESCRT-III (SNF7, VPS, ALIX) multiprotein complexes that constrict membranes to form intraluminal vesicles [62]. The Qa-SNARE syntaxin SYP122 resides at the plasma membrane and mediates in the final stages of secretion [107].

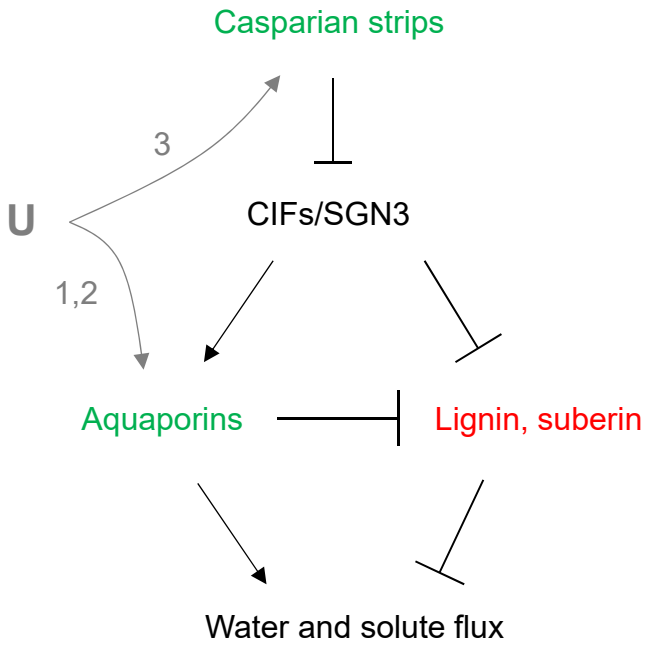

Figure S9. Hypothetical mechanisms regulating the abundance and activity of aquaporins in U-treated Arabidopsis roots.
Uranium could regulate PIP aquaporin abundance and activity by acting directly (1) at the transcriptional level, (2) at the post-translational level, and/or (3) indirectly through the CIFs/SGN3 surveillance pathway involved in sensing the integrity of the Casparian strip-based apoplastic diffusion barrier at the endodermis. CIF peptides are normally retained in the stele and do not diffuse through the apoplast where SGN complex is present. In plants impaired in Casparian strips, CIF peptides leak out between the endodermal cells and can interact with the LRR-RLK receptor SGN3, triggering a signal cascade activation leading to ectopic deposition of lignin and suberin to seal the barriers. Additionally, the activity of aquaporins is inhibited in Casparian strip and suberin deficient Arabidopsis mutants. Overall, this integrated response aims to limit the uncontrolled uptake and backflow of solutes across the root and vascular tissues to mitigate the loss of Casparian strip integrity and to ensure relatively normal plant growth and development. This model is based on [93–96]. This physiological response could be activated in presence of U as CASP proteins and several PIP aquaporins are down-accumulated (shown in green) while lignin and suberin synthesizing proteins are up-accumulated (in red) (see details in Figure 6). Ectopic lignin deposition was observed in Arabidopsis root under U stress [16].